

The effect of climate change on the simulated streamflow of six Canadian rivers based on the CanRCM4 regional climate model

Vivek. K. Arora¹, Aranildo Lima¹, Rajesh Shrestha²

¹Canadian Centre for Climate Modelling and Analysis, Climate Research Division, Environment Canada, Victoria, BC, Canada

²Climate Research Division, Environment and Climate Change Canada, Victoria, BC, Canada

1

2 *Correspondence to:* Vivek K. Arora (vivek.arora@ec.gc.ca)

3 **Abstract**

4

5 The effect of climate change on the hydro-climatology, in particular streamflow, of six major
6 Canadian rivers (Mackenzie, Yukon, Columbia, Fraser, Nelson, and St. Lawrence) is investigated,
7 by analyzing results from the historical and future simulations (RCP 4.5 and 8.5 scenarios)
8 performed with the Canadian regional climate model (CanRCM4). Streamflow is obtained by
9 routing runoff using river networks at 0.5° resolution. Of these six rivers, Nelson and St. Lawrence
10 are the most regulated. As a result, the streamflow at the mouth of these rivers shows very little
11 seasonality. Additionally, the Great Lakes significantly dampen the seasonality of streamflow for
12 the St. Lawrence River. Mean annual precipitation (P), evaporation (E), runoff (R), and
13 temperature increase for all six river basins in both future scenarios considered here, and the
14 increases are higher for the more fossil fuel-intensive RCP 8.5 scenario. The only exception is the
15 Nelson River basin for which the simulated runoff increases are extremely small. The hydrological
16 response of these rivers to climate warming is characterized by their existing climate states. The
17 northerly Mackenzie and Yukon River basins show a decrease in evaporation ratio (E/P) and an
18 increase in runoff ratio (R/P) since the increase in precipitation is more than enough to offset the
19 increase in evaporation associated with increasing temperature. For the southerly Fraser and
20 Columbia River basins, the E/P ratio increases despite increase in precipitation, and the R/P ratio
21 decreases due to an already milder climate in the Pacific north-western region. The seasonality
22 of simulated monthly streamflow is also more affected for the southerly Fraser and Columbia
23 Rivers than for the northerly Mackenzie and Yukon Rivers as snow amounts decrease and
24 snowmelt occurs earlier. The streamflow seasonality for the Mackenzie and Yukon rivers is still
25 dominated by snowmelt at the end of the century even in the RCP 8.5 scenario. The simulated
26 streamflow regime for the Fraser and Columbia Rivers shifts from a snow-dominated to a
27 hybrid/rainfall-dominated regime towards the end of this century in the RCP 8.5 scenario. While
28 we expect the climate change signal from CanRCM4 to be higher than other climate models,
29 owing to the higher-than-average climate sensitivity of its parent global climate model, the
30 results presented here provide a consistent overview of hydrological changes across six major
31 Canadian river basins in response to a warmer climate.

32

Deleted: is investigated

Deleted: ,

Deleted: in particular streamflow,

Deleted: considered

37 **1. Introduction**

38 As the global population and the standard of living increases so does the strain on
39 freshwater resources. The natural availability of water is determined by the balance between
40 precipitation (P) and evaporation (E) (this includes both evaporation and transpiration from
41 plants). When precipitation exceeds evaporation, which is determined primarily by available
42 energy, the water that does not evaporate or transpire (either at the surface or after infiltration
43 into the soil) termed runoff (R) is carried by the rivers to the oceans. The seasonality of
44 precipitation, its partitioning into snow and rainfall, and the seasonality of snowmelt and
45 evaporation, all of which are determined by the climate in a given catchment or river basin
46 eventually determine the seasonality of runoff. As anthropogenic climate change progresses,
47 changes in the mean annual amounts and the seasonality of these different water budget
48 components will lead to corresponding changes in runoff (Trenberth et al., 2007). Changes in
49 precipitation extremes are also expected to lead to corresponding changes in the extremes of
50 streamflow. The changes in streamflow have implications for floods and power generation. While
51 runoff is expressed in similar units to precipitation and evaporation (depth of water per unit time,
52 e.g. mm/s or m/year), streamflow is the volume of water generated per unit time (e.g. m³/s or
53 km³/year) and requires multiplication with the area over which runoff is generated. Streamflow
54 is also routed down the river network which introduces a time lag and attenuation of the peak
55 runoff.

Deleted: although the term evapotranspiration is more correct...

Deleted: '

Deleted: a

Deleted: As a result, the streamflow is expressed in units of volume per unit time (e.g. m³/s or km³/year).

56 Output from climate and Earth system models (ESMs) remains the primary source of
57 information for evaluating climate change impacts. Current approaches that rely on information
58 generated by ESMs, to obtain an estimate of how future streamflow may potentially change, may

65 be classified into two broad categories. The first approach uses simulated runoff directly from
66 the land surface component of single or multiple climate models which may be routed
67 downstream to obtain streamflow at the mouths of river basins and at different points along a
68 given river network (Arora and Boer, 2001; Miller and Russell, 1992; Zhang et al., 2014). Using
69 direct runoff output from climate models has the benefit that the calculated changes in runoff
70 are physically consistent with the altered radiative balance of the Earth in response to increases
71 in the concentrations of greenhouse gases (GHGs). The corresponding changes in the general
72 circulation of the atmosphere result in the associated changes in near-surface temperature,
73 precipitation, and the hydrological cycle. ~~However, this approach suffers from three limitations~~
74 – 1) the biases in the climate simulated by the climate model, 2) the fact that the land surface
75 components of climate models are not calibrated for a given river basin but rather designed to
76 operate in a reasonably realistic way over the whole globe, and 3) the coarse resolution of global
77 climate models (GCMs). The last limitation is partially addressed when data from finer-resolution
78 regional climate models is used. The biases in the simulated climate do affect the simulated
79 runoff for the current climate. ~~Despite this, the approach can effectively capture the effects of~~
80 ~~climate change including increased evaporative demand~~ (Winter and Eltahir, 2012), ~~reduced~~
81 ~~snowpack~~ (Salathé et al., 2010; Shrestha et al., 2021a), ~~increased winter streamflow, and earlier~~
82 ~~snowmelt-driven peak flow~~ (L. Sushama et al., 2006; Poitras et al., 2011). The second approach
83 attempts to overcome these limitations by downscaling and/or bias-correcting climate from
84 climate models for future scenarios and uses that to drive a well-calibrated hydrological model
85 for given catchments or river basins (Gosling et al., 2011; Ismail et al., 2020; Miller et al., 2021;
86 Yoosefdoost et al., 2022). The second approach is more prevalent for watershed to regional scale

Deleted: T

Deleted: however,

Deleted: e second

Deleted: response to

Deleted: climate change signals

Deleted: ,

Deleted: such

Deleted: as

Deleted: (Winter and Eltahir, 2011)

Deleted: (Salathe et al. 2010; Shrestha et al. 2021)

Deleted: (Sushama et al. 2006; Poitras et al. 2011).

Deleted: is relatively robust and there is useful information in the simulated change

Deleted: that can be used to inform adaptation measures

Formatted: French (Canada)

101 impacts and adaptation studies. Given the large effort involved in downscaling and bias-
102 correcting raw climate data from climate models, most current impact studies use downscaled
103 and bias-corrected data put together by other groups rather than specifically doing this for their
104 project. Recent examples include the downscaled and bias-corrected climate data for the
105 conterminous United States (Thrasher et al., 2013) based on climate model output from the fifth
106 phase of the Coupled Model Intercomparison Project (CMIP5), and statistically downscaled and
107 bias-corrected data from five CMIP5 models, available at the global scale, tailored to the
108 requirements of the Inter-Sectoral Impact Model Intercomparison Project (ISIMIP) (Lange, 2019).

Deleted: based

109 Both these data sets have found large applications in the impacts and adaptation community.
110 The processes of downscaling and bias correction are distinct, and they both have their inherent
111 limitations. There are several examples of the limited ability of bias-correction to correct and to
112 downscale variability, and that bias-correction can potentially cause implausible climate change
113 signals (Maraun, 2016; Maraun et al., 2017). There are also uncertainties, substantial
114 contradictions, and sensitivity to assumptions between the different downscaling methods
115 (Hewitson et al., 2014).

Deleted: dataset

Deleted: ,
Deleted: and t
Deleted: remain

116 Finally, while land surface models are typically used within the coupled framework of
117 climate models, hydrological models that are typically used as a standalone model for impact
118 studies. While the primary output quantities from hydrological models are runoff and
119 streamflow, land surface models output a range of water, energy, and CO₂ fluxes. The layer of air
120 directly above the land surface, commonly referred to as the atmospheric or planetary boundary
121 layer, is affected by surface-atmosphere exchanges of energy and water and extends upward
122 into the atmosphere. A realistic representation of turbulent fluxes of energy and water in the

Moved down [1]: Furthermore, setting up and calibration of a hydrologic model for a large region like Canada by correctly representing regulation, and projecting future climate impacts by downscaling and bias correcting ensemble of GCMs is very a challenging task, and that is why it has only been done for a selected few river basins in Canada and that too considering one river basin at a time.

Deleted: there are differences in
Deleted: used for the first approach and
Deleted:
Deleted: in the second approach
Formatted: Subscript

Deleted: n
Deleted: accurate

141 planetary boundary layer is essential to the transport of moisture and energy through the
142 atmosphere. As a result, while calibration of hydrological models to reproduce observed
143 streamflow is a routine exercise (Chegwidden et al., 2019; Hattermann et al., 2018; Huang et al.,
144 2020; Hundecha et al., 2020), land surface models cannot be calibrated to reproduce a single or
145 a small subset of quantities. Rather land surface models are expected to reproduce reasonably
146 realistic estimates of a range of energy, water, and CO₂ fluxes over the whole globe. The
147 philosophy behind land surface models, as they are used in the context of climate models, is that
148 given 1) a model's structure and parameterizations, 2) the driving geophysical data for fields such
149 as vegetation cover, soil depth, and soil texture, and 3) the driving meteorological variables, a
150 model is expected to reasonably realistically reproduce various components of the water,
151 energy, and carbon cycle at the global scale. The global scale of land surface models within the
152 framework of climate models precludes tuning of their parameters for individual grid cells or for
153 a region (e.g. a river basin) to reproduce a small subset of model outputs.

154 While well-calibrated hydrological models are generally suitable for a given catchment or
155 a river basin their application cannot be easily extended to large-scale global or regional
156 hydrologic modelling studies since it is typically not feasible to tune model parameters for all grid
157 cells in a large domain. For a large region like Canada correctly representing anthropogenic
158 regulation, using downscaled and bias corrected climate data from an ensemble of climate
159 models is a challenging task, and that is why it has only been done for a selected few river basins
160 in Canada and that too considering one river basin at a time. In the end, both approaches have
161 their strengths and limitations for assessing climate change impacts on hydrology and can be
162 considered complementary to each other.

- Deleted: (References)
- Deleted: budget
- Formatted: Subscript
- Deleted: the
- Deleted: and
- Deleted: in the form of the geographical distribution geophysical ...
- Deleted: physical
- Deleted: (
- Deleted:)
- Deleted: geographical distribution of
- Deleted: aspects
- Deleted: use
- Deleted: A land surface model's parameters cannot be
- Deleted: ed
- Deleted: For this reasonw
- Deleted:
- Deleted: For example, moisture resulting from evaporation calculated by a land surface model (or equivalently latent heat flux, in energy units), when coupled to an atmospheric model, is advected through the atmosphere. Net radiation at the land surface is partitioned into latent and sensible heat fluxes. When soil moisture is limiting a larger fraction of net radiation is partitioned into
- Deleted: W
- Deleted: but
- Deleted: has not
- Deleted: been
- Deleted: straightforward
- Deleted: river basins
- Moved (insertion) [1]
- Deleted: Furthermore, setting up and calibration of a hydrologic model f...
- Deleted: by
- Deleted: and
- Deleted: projecting future climate impacts by
- Deleted: ing
- Deleted: ing
- Deleted: GCMs
- Deleted: very
- Deleted: are

202 Future hydrologic projections using the second approach (hydrological modes driven by
203 statistically downscaled and bias-adjusted climate models) are available for selected river basins
204 in Canada. The results over the Prairies and British Columbia (Shrestha et al., 2021b; Sobie and
205 Murdock, 2022) generally indicate shorter snow cover duration, earlier snowmelt, and reduced
206 annual maximum snow water equivalent as the climate warms. Streamflow projections across
207 Canada generally indicate earlier snowmelt-driven peak flow, increased winter flow, and
208 decreased summer flow (Budhathoki et al., 2022; Dibike et al., 2021; Islam et al., 2019;
209 MacDonald et al., 2018; Shrestha et al., 2019). Annual streamflow is projected to increase, with
210 higher increases in the northern basins (Bonsal et al., 2020; Stadnyk et al., 2021). However, these
211 projections are based on different climate and hydrological models, downscaling methods,
212 emissions scenarios, and future periods, and no consistent set of projections is available across
213 all major river basins of Canada.

Deleted: ¶

Deleted: occurring

Formatted: French (Canada)

Deleted: generally

214 In this study, we have used the first approach to provide a consistent set of projections
215 across all major river basins of Canada, while being cognizant of its limitations. We investigate
216 the effect of climate change on the annual, monthly, and daily streamflow characteristics of six
217 major Canadian rivers (Mackenzie, Yukon, Columbia, Fraser, Nelson, and St. Lawrence) using
218 runoff output from simulations performed with version 4 of the Canadian Regional Climate
219 Model (CanRCM4) (Scinocca et al. 2016). The river basins of the Yukon and Columbia Rivers cover
220 part of the United States of America as well. We used daily runoff generated from CanRCM4 for
221 the historical period and for the two future scenarios (representative concentration pathways
222 (RCP) 4.5 and 8.5). The spatial resolution of runoff data from CanRCM4 is 0.22° which is
223 equivalent to about 12 km at 60° N (Canada lies between approximately 42°N and 83°N). We

Deleted: .

Deleted: Additionally, we utilized a large ensemble (50 realizations) of the CanRCM4 (CanRCM4-LE) at 0.44° resolution to quantify uncertainties associated with internal variability. ...

232 then routed this runoff through river networks at 0.5° resolution to evaluate streamflow at the
233 mouths of major Canadian rivers. The Mackenzie, Yukon, and Fraser Rivers are somewhat less
234 regulated than the heavily regulated Nelson, Columbia, and St. Lawrence Rivers. The routing
235 scheme used here does not take into account dams and reservoirs and therefore the modelled
236 streamflow represents natural streamflow. This aspect is discussed in more detail in Section 2.

Deleted: 0

237 2. Models and data

Formatted: Indent: First line: 0 cm

238 Equation (1) summarizes the water balance over a given grid cell or a river basin for a
239 given timescale.

$$240 \quad P = E + R + \Delta S \quad (1)$$

241 where ΔS is the change in water storage including that in soil moisture, snow, and the canopy
242 water storage. All terms are expressed in depth per unit time units (e.g. mm/year). When a
243 system is in equilibrium, at annual or longer timescales $\Delta S = 0$ and $P = E + R$. ΔS , however,
244 may not be zero even over long timescales when a system is not in equilibrium e.g., when snow
245 is accumulating or is melting consistently. We evaluated the P, E, and R components of equation
246 (1) simulated by CanRCM4 for each of the six river basins, considered in this analysis, and routed
247 R to obtain streamflow at the river mouths.

Deleted: combined

248

249 2.1 The Canadian Regional Climate Model (CanRCM4)

250 CanRCM4 uses the fourth-generation Canadian atmospheric physics (CanAM4) package
251 (von Salzen et al., 2013), which is the product of a multi-decadal program of climate model
252 development at the Canadian Centre for Climate Modelling and Analysis (CCCma), a section

255 within Environment and Climate Change Canada. The CanAM4 atmospheric physics package is
256 also used in CanESM2 (Arora et al., 2011) which contributed results to CMIP5. The difference
257 between CanRCM4 and CanESM2, other than the former being a regional climate model and the
258 latter being a comprehensive global ESM, is that CanRCM4 employs the limited-area
259 configuration of the Global Environmental Multiscale (GEM) model (Côté et al., 1998), which uses
260 a semi-Lagrangian dynamical core for advection in the atmosphere and is developed by
261 Environment and Climate Change Canada's Recherche en Prévision Numérique (RPN) where it is
262 used both for global and regional numerical weather prediction. CanESM2 on the other hand
263 uses a spectral dynamical core for advection in the atmosphere. CanRCM4 is driven at its
264 boundaries with data from its parent model (CanESM2). An overview and technical details of the
265 coordinated global and regional climate modelling effort used to develop the CanESM2-CanRCM4
266 system are described in detail by Scinocca et al. (2016). Results from the model's North American
267 0.22° domain, for a single ensemble member, are primarily used here. In addition, we also used
268 runoff from CanRCM4 0.44° resolution simulations for the North American domain because of
269 the availability of a large ensemble (LE) of 50 members (CanRCM4 LE) (ECCC, 2018). The large
270 ensemble simulations allow the consideration of CanRCM4's internal variability, which is an
271 intrinsic property of the climate system and models, that is largely irreducible and could account
272 for a large fraction of the inter-climate model spread (Deser et al., 2020). The results used here
273 from CanRCM4's form part of its contribution to the coordinated regional climate downscaling
274 experiment (CORDEX) effort. The North American domain of CanRCM uses a rotated latitude-
275 longitude projection with the North Pole at longitude 83° E and latitude 42.5° N, as opposed to
276 the geographic North Pole (longitude 0°E, latitude 90° N).

Deleted: the

Deleted: GCM

279 The land surface component in CanAM4 is the coupled CLASS-CTEM model. The physical
280 processes are based on the Canadian Land Surface Scheme (CLASS) (Verseghy, 1991; Verseghy et
281 al., 1993), and biogeochemical processes (which simulate vegetation as a dynamic component of
282 the climate system) are based on the Canadian Terrestrial Ecosystem Model (CTEM) (Arora and
283 Boer, 2003, 2005). The configuration of CLASS-CTEM used in CanESM2 and CanRCM4 uses three
284 soil layers with thicknesses of 0.10, 0.25, and 3.75 m. Liquid and frozen soil moisture contents,
285 and soil temperature, are determined prognostically for the three soil layers. The temperature,
286 albedo, mass, and density of a single layer snow pack (when environmental conditions permit
287 snow to exist) are also prognostically modelled. Surface runoff is generated in CLASS when
288 precipitation intensity exceeds infiltration capacity and when the top soil layer is saturated. The
289 rainwater and snow melt that infiltrate, the soil are available for soil evaporation and
290 transpiration. Any remaining water percolates down the soil profile and comes out at the bottom
291 of the soil profile and is termed drainage. Combined surface runoff and drainage constitute total
292 runoff. Like most land surface components of ESMs, CLASS does not include a groundwater
293 representation. Surface runoff and drainage from CLASS are used as input into a large-scale river
294 routing scheme to route runoff and obtain streamflow at the mouth of the rivers considered in
295 this study as explained in the next section.

Deleted: the physics component of

Deleted: single-layer

Deleted: s

Deleted: is

Deleted: components of runoff

296 2.2 Variable velocity routing model

297 The variable velocity river routing scheme of Arora and Boer (1999) that is implemented
298 in the family of Canadian ESMs (CanESMs) (Arora et al., 2009, 2011; Swart et al., 2019) is used to
299 route daily runoff from CanRCM4. This routing scheme has been implemented in various versions
300 of CanESMs at a spatial resolution of 2.81° since the year 2000. For this study, the routing scheme

306 was implemented at a spatial resolution of 0.5°. The reason for using river routing at 0.5°
307 resolution instead of scaling river networks to the 0.22° rotated latitude-longitude projection of
308 CanRCM4 's North American domain is that scaling river networks is a non-trivial and
309 cumbersome task that cannot be fully automated (Arora and Harrison, 2007). In contrast,
310 conservatively regridding runoff from one spatial resolution to another is a straightforward
311 process. In addition, it has been shown that routing is not very sensitive to the spatial scale at
312 which it is performed. Specifically, Arora et al. (2001) evaluated the Arora and Boer (1999) routing
313 scheme together with the WATROUTE routing scheme at ~350 km and ~25 km spatial resolutions,
314 respectively, for the Mackenzie River basin. The two routing schemes were driven with the same
315 runoff. Arora et al. (2001) conclude that for the purpose of realistically modelling streamflow at
316 the mouth of the rivers in climate models, flow routing at large spatial scales gives similar results
317 to routing at finer spatial scale. In our study the difference between the spatial resolution of
318 runoff (0.22° and 0.44°) from the CanRCM4 model and routing (0.5°) is much smaller than the
319 Arora et al. (2001) study. As a result, we do not expect that routing at a slightly different spatial
320 resolution than runoff will lead to significant differences in the simulated streamflow. The
321 routing scheme needs river flow directions and these are obtained from the Total Integrating
322 Runoff Pathways (TRIP) data set ([http://hydro.iis.u-](http://hydro.iis.u-tokyo.ac.jp/~taikan/TRIPDATA/TRIPDATA.html)
323 [tokyo.ac.jp/~taikan/TRIPDATA/TRIPDATA.html](http://hydro.iis.u-tokyo.ac.jp/~taikan/TRIPDATA/TRIPDATA.html), last accessed July 2023) of Oki and Sud (1998).
324 The TRIP data are available at the regular latitude-longitude grid with the geographic North Pole
325 at its usual location (0° E, 90° N). Figure 1 shows the river networks at 0.5° resolution based on
326 TRIP data which also identifies the six river basins investigated in this study. The Fraser River
327 (identified by the light green colour) appears to have a river mouth over land. This is because the

Deleted: has been shown to be
Deleted: scale
Deleted:
Deleted: (
Deleted: ,

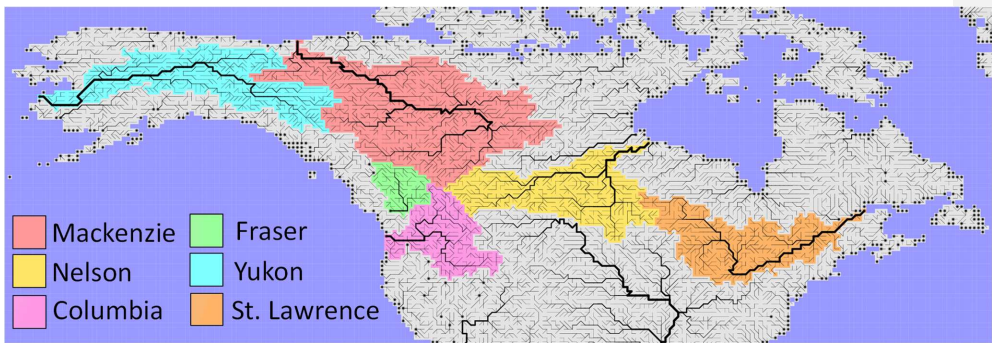
Deleted: scale
Deleted: the spatial scale of
Deleted:
Deleted: performing

Deleted: scale
Deleted: bias
Deleted: in any significant manner

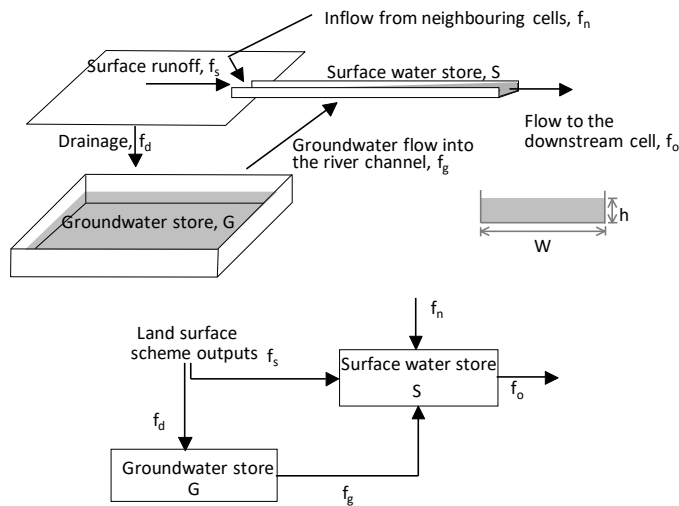
Deleted: dataset
Deleted:

342 Fraser River drains into the narrow Strait of Georgia which is not resolved at the 0.5° resolution
 343 of the TRIP [data set](#). In addition, the TRIP data set does not resolve any inland lakes and provides
 344 river flow directions over grid cells that are lakes. This is in fact helpful because it avoids
 345 discontinuities in the river network.

Deleted: dataset



346
 347 **Figure 1:** River flow networks at 0.5° resolution used in this study. The major river basins for
 348 which streamflow and runoff are analyzed in this study are also identified.



349
 350

Deleted: ¶

353 **Figure 2:** Schematic of the Arora and Boer (1999) river routing scheme used in this study to route
 354 runoff simulated by CanRCM4.

356 Figure 2 shows the schematic of the routing scheme which uses surface runoff and
 357 drainage outputs from the land surface scheme. The variable velocity routing scheme used here
 358 is described briefly below and more details can be found in Arora and Boer (1999). The water
 359 balance within a grid cell for its surface S (m^3) and groundwater G (m^3) stores is given by

$$\frac{dS}{dt} = f_s + f_n + f_g - f_o \quad (2)$$

$$\frac{dG}{dt} = f_d - f_g \quad (3)$$

362 where, f_s and f_d are the surface runoff and drainage (or baseflow) estimates given by the land
 363 surface scheme, f_n and f_o are the surface water inflow from the adjacent upstream neighbouring
 364 grid cell(s) and outflow to the downstream grid cell respectively, and f_g is the groundwater
 365 outflow from the groundwater reservoir to the surface water reservoir within a grid cell as shown
 366 in Figure 2. The fluxes are represented in m^3/s .

367 A river channel is assumed to be rectangular and the width (W) of the river at every point
 368 along the river network is specified a priori. This river width in meters is calculated based on its
 369 geomorphological relationship with mean annual discharge. The surface runoff contributes
 370 directly to the surface water store which is essentially the amount of water in the rectangular
 371 river channel between two grid cells. The flow velocity (V , m/s) is calculated using the Mannings
 372 formula (Manning, 1891).

$$V = \frac{1}{n} R^{2/3} S^{1/2} = \frac{1}{n} \left(\frac{A}{P} \right)^{2/3} n^{1/2} = \frac{1}{n} \left(\frac{Wh}{W+2h} \right)^{2/3} n^{1/2} \quad (4)$$

Deleted: here

Formatted: Font: Italic

Formatted: Superscript

Formatted: Font: Italic

Formatted: Superscript

Deleted:

Formatted: Right

Formatted: Font: Italic

Formatted: Font: Italic, Subscript

Formatted: Font: Italic

Formatted: Font: Italic, Subscript

Formatted: Font: Italic

Formatted: Font: Italic, Subscript

Formatted: Font: Italic

Formatted: Subscript

Formatted: Font: Italic

Formatted: Subscript

Deleted: In

Formatted: Superscript

Deleted: The

Deleted: s

Deleted: s

Deleted: 2

381 where r is the unitless Mannings roughness coefficient (a default value of 0.04 is used), A is the
 382 area of the river channel (m^2), P is the wetted perimeter (m), and h is the depth of water in the
 383 channel (m). The slope n (unitless) of the channel is calculated using elevation difference and the
 384 river length between two grid cells.

385 The river channel storage S is assumed to be a linear function of outflow discharge, so

$$386 \quad S = \tau f_o = \frac{L}{V} AV = LA = LWh \quad (5)$$

387 where τ is the travel time between the grid cell under consideration and its downstream
 388 neighbor given by $\tau = L/V$, where L is the distance between the grid cells (m). The outflow f_o is
 389 given by

$$390 \quad f_o = AV = WhV = Wh \frac{1}{r} \left(\frac{Wh}{W+2h} \right)^{2/3} n^{1/2} \quad (6)$$

391 and substituting (5) and (6) into (2) yields

$$392 \quad \frac{dh}{dt} = \frac{1}{LW} \left(I - \frac{W^{5/3} h^{5/3}}{r(W+2h)^{2/3}} n^{1/2} \right) \quad (7)$$

393 where I (m^3/s) is the total inflow into a grid cell ($I = f_s + f_n + f_o$). Equation (7) describes the flow in
 394 terms of the rate of change of flow depth for a given river section. An explicit forward step finite
 395 difference approximation for (7) yields

$$396 \quad h(t+1) = h(t) + \frac{\Delta t}{LW} \left(I(t) - \frac{W^{5/3} h(t)^{5/3}}{r(W+2h(t))^{2/3}} n^{1/2} \right) \quad (8)$$

397 Flow velocity and outflow discharge for the river channel at any time step can be obtained using
 398 equations (4) and (6). For the 0.5° resolution used here, stable solution of (8) is obtained with Δt

Formatted: Superscript

Formatted: Font: Not Italic

Formatted: Indent: First line: 1.27 cm

Formatted: Font: 14 pt

Deleted: ?

Formatted: Font: Italic

Formatted: Font: Italic

Formatted: Font: Italic, Subscript

Deleted: ?

Formatted: Font: Italic

Formatted: Superscript

Formatted: Font: Italic

Formatted: Font: Italic

Formatted: Font: Italic, Subscript

Formatted: Font: Italic

Formatted: Font: Italic, Subscript

Formatted: Font: Italic

Formatted: Font: Italic, Subscript

401 equal to around 10 minutes. The approach yields dynamically-varying flow depth, velocity, and
402 discharge through the river channel in response to changing surface and baseflow runoff inputs
403 from the land surface model.

404 The groundwater component of the routing model assumes that groundwater storage, G ,
405 is a linear function of groundwater outflow, f_g .

$$G = \tau_g f_g \quad (9)$$

407 The delay in the groundwater store (τ_g) is based on the dominant soil texture type and is set to
408 10, 35, and 65 days if the dominant soil type in each grid cell is sand, silt, and clay, respectively,
409 following Arora and Boer (1999). Substituting G in equation (3) yields,

$$\tau_g \frac{df_g}{dt} = f_d - f_g \quad (10)$$

411 and following Arora and Boer (1999) we use the following expression

$$f_g(t + 1) = f_g(t) e^{-\Delta t/\tau_g} + \left(1 - e^{-\frac{\Delta t}{\tau_g}}\right) f_d(t) \quad (11)$$

413 to determine discharge from the groundwater reservoir within a grid cell and to step forward in
414 time, where a time step Δt equal to three hours is used. The simplistic form of equation (11)
415 allows to use a much larger time step than the time step of 10 minutes required for equation (8).

416 The routing scheme used here does not consider the flow regulation effect of dams and
417 reservoirs. It, however, does consider the effect of lakes and ice jams in a simple manner. The
418 global lake data set from Kourzeneva et al. (2012) is used which prescribes the fractional coverage
419 of sub-grid lakes and the five Laurentian Great Lakes (Lakes Superior, Michigan, Huron, Ontario,

Formatted: Font: Italic

Formatted: Indent: First line: 1.27 cm

Formatted: Font: Italic

Formatted: Font: Italic, Subscript

Deleted: Multiplied with the river's cross-sectional area, the time-varying velocity determines the output discharge from the surface water store of the current grid cell to the river channel of the downstream grid cell. The drainage from the bottommost soil layer contributes to the groundwater store which eventually contributes to the surface water store in the same grid cell. ...

Deleted: Both the depth and velocity of the water in the river channel are prognostic variables and evolve in dynamically change over time depending on the amount of water in the a river channel.

431 and Erie). In particular, the flow at the mouth of the St. Lawrence River is affected significantly
432 by the Great Lakes. The hydraulic residence [time](#) of water in the Great Lakes varies from about 2
433 years for Lake Erie to about 200 years for Lake Superior (Quinn, 1992). As a result, even in the
434 absence of anthropogenic flow regulation for the St. Lawrence River, we expect the streamflow
435 at its mouth to show very little seasonality compared to the usual spring peak of Canadian rivers
436 dominated by snowmelt. The simple approach used here delays the streamflow flowing into a
437 grid cell with a lake fraction greater than 60% using an e-folding time scale of 300 days similar to
438 the treatment of the groundwater reservoir (Figure 2) (Arora and Boer, 1999). For the St.
439 Lawrence River, the effect of delay caused by the Great Lakes is much larger than that of the
440 anthropogenic flow regulation.

441 Ice jams and breakups are complex thermal and mechanical events and therefore
442 challenging to model. They occur on all Canadian rivers with varying degrees and depend on
443 winter temperatures, the river bathymetry, and the physical and geomorphological conditions of
444 rivers (Beltaos, 2000; Prowse, 1986). The winter freezing of river water inevitably leads to a slow
445 down of river flow velocity. When water cannot move downstream, upstream flooding results.

446 Here, we have used a simple approach that increases Manning's roughness coefficient for the
447 Mackenzie and the Yukon Rivers (which are the most northerly and therefore affected the most
448 by ice jams) for the period January to June. The value of Manning's roughness coefficient is
449 increased linearly from 0.04 to 0.08 from 1 January to 31 January, kept at 0.08 from 1 Feb to 31
450 May, and then reduced linearly from 0.08 to 0.04 over the period June 1 to 30 June. Chen and
451 She (2020) report the trend in river ice breakup dates for the Mackenzie and Yukon Rivers to be
452 around -0.3 and -1.3 days/decade for the 1950-2016 period, where the negative sign indicates

Deleted: (a value of 0.08 is used)

454 that the ice breakup is occurring earlier. Assuming the same trend, the breakup dates would
455 occur about 2.5 and 11 days earlier towards the end of this century, respectively, for the
456 Mackenzie and Yukon rivers. This simple approach reduces the river flow velocity during the
457 months that are most affected by river ice jams. Although this is not a perfect nor a complete
458 approach this simple treatment allows to improve the streamflow seasonality for the Mackenzie
459 and Yukon rivers. For the southerly Fraser and Columbia rivers such treatment was not necessary.
460 Consideration of a higher roughness coefficient for the St. Lawrence River to account for ice jams
461 does not affect its streamflow's seasonality (or rather the lack of it) which is overwhelmingly
462 determined by the delay and storage caused by the Great Lakes.

Deleted: n't

463 2.3 Modelled and observation-based data

464 The CMIP5 historical simulation covers the period 1850-2005 and the future scenarios
465 cover the period 2006-2100. We used daily runoff from CanRCM4 from its 0.22° North American
466 domain for the 20-year period 1986-2005 from one ensemble member of the historical
467 simulation and for the 20-year period 2081-2100 from one ensemble member each for the two
468 future scenarios (RCP 4.5 and RCP 8.5, Moss et al. (2010)). The RCP 8.5 is the highest baseline
469 emissions scenario where future development is based on continuous fossil-fuel development.
470 As a result, CO₂ emissions and concentrations increase throughout the 21st century and CO₂
471 concentration in the year 2100 is around 1100 ppm. RCP 4.5 is a moderate emissions scenario in
472 which emissions peak around 2040 and then decline: as a result CO₂ somewhat stabilizes to
473 around 550 ppm by the year 2100. Since the CanRCM4 data are available on a rotated latitude-
474 longitude grid and the river routing is performed on a regular latitude-longitude grid (following
475 the TRIP data), the runoff data from CanRCM4 are conservatively regridded to the global 0.5°

Deleted: 20

Deleted: s

Deleted: 20

Deleted: s

481 grid using climate data operators (CDO)
482 (<https://code.mpimet.mpg.de/projects/cdo/embedded/index.html#x1-7170002.12.5>, last
483 accessed Dec 2023) as mentioned earlier. These runoff data are then used as input into the
484 routing model. The 20-year runoff data (1986-2005 for the historical simulation, and 2081-2100
485 for the future scenarios) are concatenated into a 40-year time series for each simulation
486 (historical, RCP 4.5, and RCP 8.5). These data are then input into the routing model and the last
487 20 years of simulated streamflow are analyzed. The 20-year spin-up is sufficient to allow the
488 surface and groundwater stores to fill up and reach equilibrium. The simulated precipitation and
489 temperature from CanRCM4 are compared against observation-based data from the CRU TS 4.07
490 product (Harris et al., 2020).

491 The simulated streamflow is compared against observation-based estimates obtained
492 from the Global Runoff Data Centre (GRDC) for the stations that are closest to the river mouths.
493 Table 1 lists the drainage areas of all rivers considered in this study as discretized in the TRIP data
494 set and at the stations closest to the river mouth. For the Columbia River, which is heavily
495 regulated, we obtain an estimate of the naturalized flow with no regulation and no irrigation
496 provided by the Bonville Power Administration (BPA) for the station VAN (near Vancouver,
497 Washington, USA) ([https://www.bpa.gov/energy-and-services/power/historical-streamflow-](https://www.bpa.gov/energy-and-services/power/historical-streamflow-data)
498 [data;https://www.bpa.gov/-/media/Aep/power/historical-streamflow-reports/historic-](https://www.bpa.gov/-/media/Aep/power/historical-streamflow-reports/historic-streamflow-nrni-flows-1929-2008-corrected-04-2017.csv)
499 [streamflow-nrni-flows-1929-2008-corrected-04-2017.csv](https://www.bpa.gov/-/media/Aep/power/historical-streamflow-reports/historic-streamflow-nrni-flows-1929-2008-corrected-04-2017.csv), last accessed July 2023). The drainage
500 area of the Columbia River upstream of the VAN station is 616960 km² and does not include
501 discharge contributions from three tributaries (Willamette, Cowlitz, and Lewis Rivers). Of these
502 three tributaries, the contribution from Willamette is the largest. We obtained naturalized

Deleted: then

504 streamflow for the Willamette River at the station SVN (drainage area 25,600 km²) also from
 505 BPA's website ([https://www.bpa.gov/-/media/Aep/power/historical-streamflow-](https://www.bpa.gov/-/media/Aep/power/historical-streamflow-reports/correction-20220801.zip)
 506 [reports/correction-20220801.zip](https://www.bpa.gov/-/media/Aep/power/historical-streamflow-reports/correction-20220801.zip), from the file SVN6ARF_daily_COR.xlsx) and added it to the
 507 naturalized streamflow at the station VAN. This yields naturalized streamflow for the entire
 508 Columbia River basin, except the smaller Cowlitz, and Lewis Rivers, and represents a drainage
 509 area of 642,560 km² (see Table 1).

510 The Nelson River is affected by two large lakes, Lake Winnipeg and Lake Manitoba, and it
 511 is also heavily regulated. It currently has five dams towards the end of its journey as it flows into
 512 Hudson Bay. There are no upstream gauging stations close to the first upstream dam. In addition,
 513 water is also diverted from Churchill to the Nelson River. We were unable to obtain naturalized
 514 flow for the Nelson River [from the Manitoba hydroelectricity company](#). Due to anthropogenic
 515 flow regulation on the Nelson River, the present-day streamflow shows very little seasonality (as
 516 shown later). As a result, we do not evaluate the simulated [daily or](#) monthly streamflow for the
 517 Nelson River and focus only on its mean annual value.

518 **Table 1:** Comparison of river basin areas as represented in the TRIP data and at the gauging
 519 station closest to the river mouth for the river basins considered in this study as obtained from
 520 the GRDC.

521

River basin	River basin area (million km ²)		Gauging station
	in the TRIP data set	at the gauging station closest to the river mouth	
Mackenzie	1.74	1.66	Arctic red river
Yukon	0.85	0.83	Pilot Station
Columbia	0.66	0.64	See section 2.3
Fraser	0.23	0.22	Hope
Nelson	1.07	1.06	Long Spruce generating station
St. Lawrence	1.11	0.77	Cornwall, Ontario

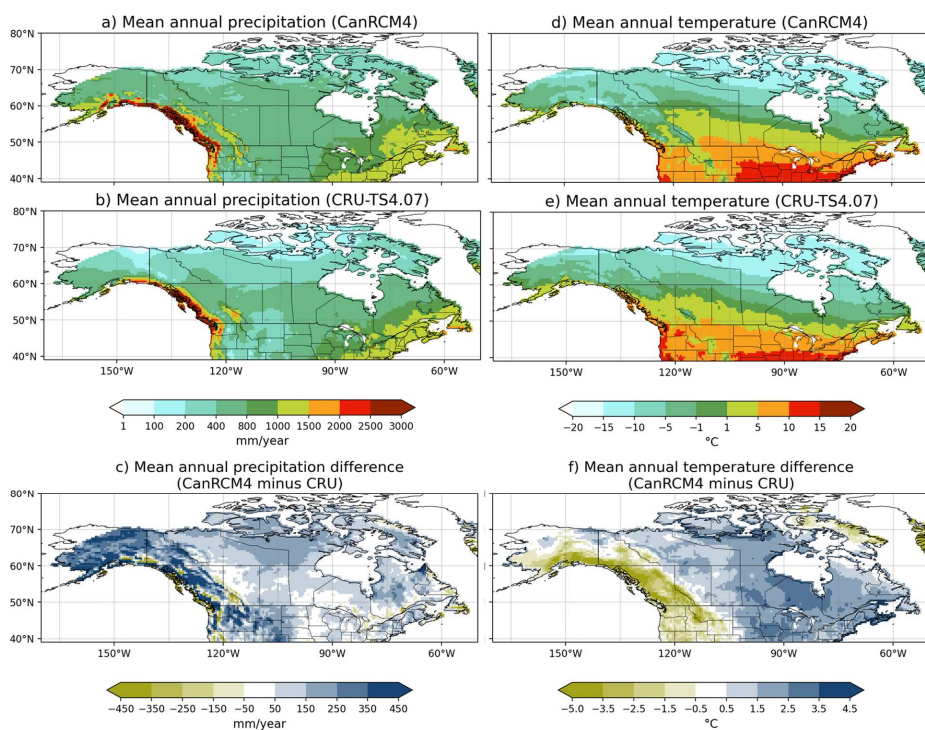
Deleted: in addition,

Deleted:

Deleted: dataset

525

526



527

528

529

530

Figure 3: Comparison of CanRCM4 simulated precipitation (left column) and temperature (right column) with observation-based estimates from the CRU TS 4.07 [data set](#) for the period 1986-2005.

531

532 3. Results

533 3.1 Present-day precipitation, temperature, and streamflow

534

535

Figure 3 compares the [geographical distribution of](#) mean annual precipitation (left column) and temperature (right column) simulated by CanRCM4 to observation-based estimates

Deleted: ¶
¶

Deleted: dataset

539 from the CRU TS 4.07 data set (referred to as CRU from here on) for the 1986-2005 period.

Deleted: dataset

540 Although the six river basins considered in this study do not cover the entire Canadian region, for
541 completeness the plots are shown for the whole of Canada and south up to 39 °N to include the
542 southern edge of the Columbia River basin. In Figure 3, while CanRCM4 broadly simulates the
543 geographical distribution of temperature and precipitation reasonably realistically, there are
544 differences compared to the CRU data set. CanRCM4 generally simulates higher precipitation

Deleted: dataset

545 over Canada and more so to the west of the Rockies (Figure 3c) compared to observations. The
546 model simulates cooler than observed temperatures to the west of the Rockies and higher than
547 observed temperatures to the east of the Rockies (Figure 3f). This is likely related to the
548 representation of topography in the model. The overall somewhat higher precipitation in
549 CanRCM4 over North America is also noted by Alaya et al. (2019) who compared probable
550 maximum precipitation (PMP) calculated using CanRCM4 data to estimates based on several
551 reanalyses. Alaya et al. (2019) concluded that among the three reanalyses they considered,
552 CanRCM4 compared best with the National Centre for Environmental Prediction's (NCEP) Climate
553 Forecast System Reanalysis.

Deleted: and compared it

Deleted: i

554 Figure 4 compares the simulated annual cycle of temperature (left column) and
555 precipitation (middle column) over the six river basins (Figure 1) selected in this study with
556 observation-based estimates from CRU. The right-hand side column compares simulated
557 streamflow for the six river basins with observation-based estimates from the GRDC. The basin-
558 averaged values of temperature and precipitation are calculated by area weighting the values in
559 the individual grid cells that lie inside a given river basin according to the TRIP data (Figure 1).
560 The plots also show the mean annual values (dashed lines) on the plot and their magnitude in

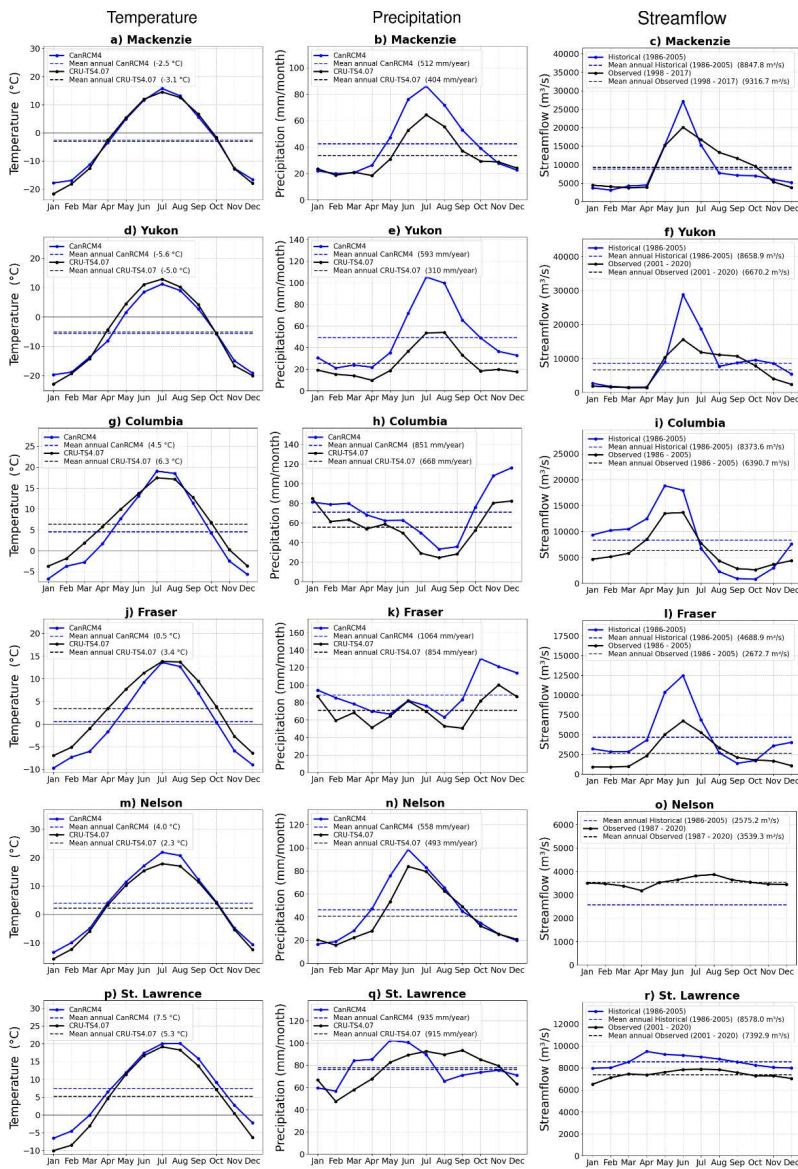
565 the legend. Figure 4 shows that overall CanRCM4 simulated basin-wide averaged temperatures
566 compare reasonably well with observation-based estimates based on the CRU data for the
567 Mackenzie and the Yukon River basins. For the Columbia and Fraser, the simulated temperatures
568 are lower for most months, and for the Nelson River basin, the CanRCM4 simulated temperatures
569 are higher compared to the CRU data. The seasonal cycle of temperature compares well with the
570 observation-based estimates from CRU data. Compared to temperature, there are larger
571 differences in simulated CanRCM4 precipitation compared to the CRU data. Although CanRCM4
572 simulates the seasonality of precipitation reasonably well compared to the CRU data, simulated
573 precipitation is higher for all river basins, consistent with Figure 3c. The comparison with the CRU
574 data provides useful insights into simulated quantities. Specifically, despite the difference in the
575 magnitudes, CanRCM4 provides a reasonable representation of the seasonality of precipitation,
576 for example higher winter precipitation in southern Fraser and Columbia basins, and higher
577 summer precipitation in northern Mackenzie and Yukon basins. However, all observation-based
578 data sets (including CRU) have their limitations. Wong et al. (2017) compared several gridded
579 observation-based precipitation data sets over Canada and found that they all have limitations
580 and the data sets compared best with gauge-based precipitation data in summer, followed by
581 autumn, spring, and winter in order of decreasing quality. Sun et al. (2018) compare global
582 precipitation from 22 gauge-, satellite-, and reanalysis-based products, including CRU, and
583 quantify the uncertainty in the different precipitation estimates over timescales ranging from
584 daily to annual. Shi et al. (2017) evaluated the CRU precipitation over large regions of China and
585 found that CRU underestimates precipitation in that region compared to rain gauge records. .
586 Furthermore, observation-based precipitation datasets also generally tend to underrepresent

Deleted: dataset
Deleted: dataset
Deleted: s
Deleted: .

591 total precipitation in mountainous western Canada (where Yukon, Mackenzie, Fraser and
592 Columbia River basins are located) due to low station density at high elevations (Werner et al.,
593 2019). In the end, the objective of the comparison of the simulated climate with CRU
594 observations is to evaluate if the model climate is reasonably realistic for the present day. The
595 assumption behind using direct output from climate models is that despite the biases in the
596 simulated current climate it is possible to deduce meaningful information about the effect of
597 climate change using the change in simulated quantities.

Deleted: (Werner et al. 2019)

598



600
 601 **Figure 4:** Comparison of the annual cycle of basin-wide averaged CanRCM4 simulated
 602 temperature (left column) and precipitation (middle column) with observation-based estimates
 603 from the CRU TS 4.07 [data set](#) for the period 1986-2005. The right-hand side column compares

Formatted: Justified, Indent: First line: 1.27 cm

Deleted: ¶

Deleted: dataset

606 simulated streamflow with observations from the GRDC. In the absence of the consideration of
607 anthropogenic flow regulation for the Nelson River only its simulated mean annual streamflow
608 value is evaluated.

609

610 The differences in simulated climate between CanRCM4 and the observation-based
611 climate in CRU for the present day affect simulated streamflow as expected. The simulated mean
612 annual streamflow is higher for four out of six river basins considered (Yukon, Columbia, Fraser,
613 and St. Lawrence) primarily because of the higher simulated precipitation. Simulated
614 precipitation is also higher for the Mackenzie River basin, but the mean annual simulated
615 streamflow compares well with its observation-based estimate. Possible reasons for reasonably
616 realistic annual simulated streamflow despite higher precipitation could be biases in the CRU
617 data set itself (e.g., underrepresentation of total annual precipitation), or higher simulated

Deleted: dataset

618 evaporation in CanRCM4 (although simulated summer temperatures compare well with the CRU
619 data). Finally, the simulated mean annual streamflow for the Nelson River is lower than its
620 observation-based estimate despite somewhat higher simulated precipitation than the CRU data.
621 The most likely reason for this is the diversion from the Churchill River into the Nelson River which
622 started in 1976 to increase the water flow to larger generating stations on the lower Nelson River.
623 The Manitoba government estimates that an average of 25% more water flows into the lower
624 Nelson River due to the Churchill River Diversion (CRD)
625 (<https://www.gov.mb.ca/sd/water/water-power/churchill/index.html>, last accessed Sep. 2023).

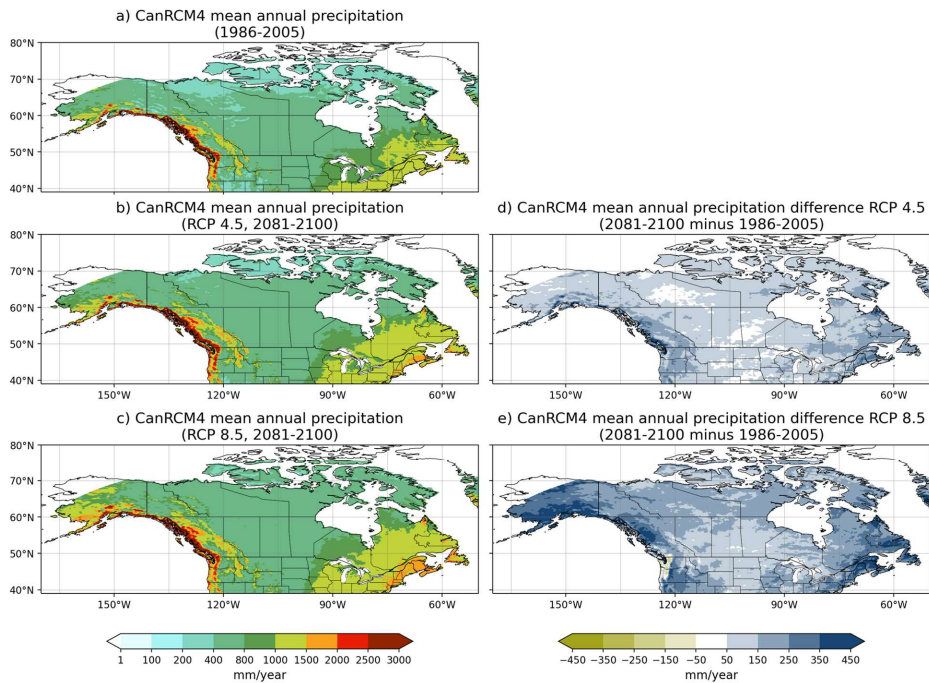
626 The seasonality of streamflow for the Mackenzie, Yukon, and Fraser Rivers is dominated by the
627 spring snowmelt with the peak occurring in June for both simulated and observed streamflow.

628 The simulated streamflow for the Columbia and Fraser rivers peaks at the right time but there is
629 more simulated streamflow during the winter months when precipitation is also higher than

631 observed. For the Mackenzie and Yukon rivers although the mean annual simulated and observed
632 streamflow are comparable their seasonal distribution is not. The simulated streamflow peak for
633 these rivers is higher due to the simple treatment of ice jams which is not sufficient to hold the
634 water in the river channel and then release it slowly as ice jams slowly dissipate in the spring and
635 summer months, as the observed streamflow indicates. Finally, for the St. Lawrence River, there
636 is little seasonality in observed streamflow due to the delay caused by the Great Lakes and
637 anthropogenic flow regulation. The lack of strong seasonality simulated in simulated streamflow
638 for the St. Lawrence River is caused entirely due to the delay caused by the Great Lakes (section
639 2.2).

640 Overall the spatial distribution of precipitation and temperature over Canada (Figure 3),
641 and the seasonality of these two primary climate drivers for the river basins considered in this
642 study (Figure 4), compare reasonably well with observation-based estimates from the CRU data,
643 although there are differences in the absolute magnitude of these variables. The resulting
644 seasonality of streamflow has limitations due to three factors: 1) the biases in the driving climate
645 from CanRCM4, 2) the biases in the land surface component of CanRCM4 which partitions
646 precipitation into evaporation and runoff, 3) the lack of calibration of the land surface component
647 to specific river basins, and 4) the lack of processes in the routing component including the
648 limitation of not being able to treat ice jams comprehensively. Despite these limitations, the
649 simulated streamflow captures the broad seasonal patterns with higher values during the spring
650 snow melt and lower values during the winter months as observations show.

651



652 **Figure 5:** Comparison of CanRCM4 simulated precipitation for the 1986-2005 and for the 2081-
 653 2100 periods, for RCP 4.5 and 8.5 scenarios.

Deleted: ,

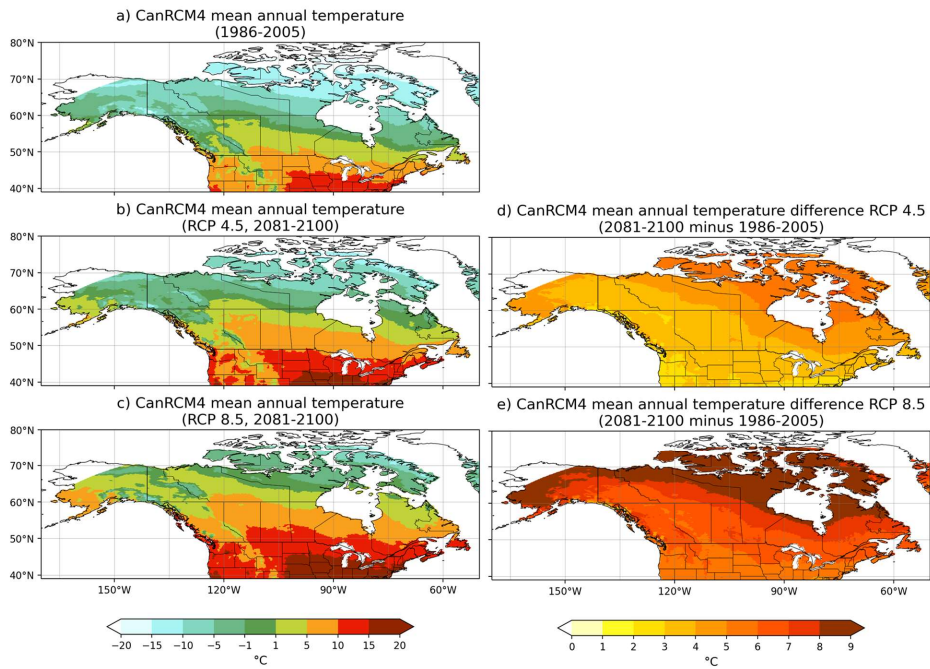
654
 655 **3.2 Changes in future climate and streamflow**

656 Figures 5, 6, and 7 show the changes in CanRCM4 simulated precipitation, temperature,
 657 and runoff for the period 2081-2100, for both RCP 4.5 and 8.5 scenarios, compared to the 1986-
 658 2005 period from the historical simulation. Over Canada, simulated precipitation and
 659 temperature increase almost everywhere and in both scenarios. As expected, the magnitude of
 660 precipitation and temperature change is higher for the RCP 8.5 than the RCP 4.5 scenario.
 661 Simulated precipitation increases are higher in the coastal western and eastern Canadian regions
 662 than in central and northern parts of Canada. The central Canadian region sees the lowest

664 increase in precipitation in both scenarios. Simulated temperature increases, as expected, are
665 higher at higher latitudes due to polar amplification of the temperature change associated with
666 the snow- and ice-albedo feedbacks. In the RCP 4.5 and 8.5 scenarios, the simulated temperature
667 changes vary from about 3 °C and 6 °C, respectively, in the south, to about 6 °C and 11 °C, in the
668 north. The parent climate model (CanESM2) on which CanRCM4 is based has an equilibrium
669 climate sensitivity of 3.7 °C, somewhat on the higher side, compared to the range of 1.5 °C to 4.5
670 °C amongst climate models that contributed to CMIP5 (Schlund et al., 2020). As a result, we also
671 expect the magnitude of simulated changes to be somewhat higher than a model with average
672 climate sensitivity.

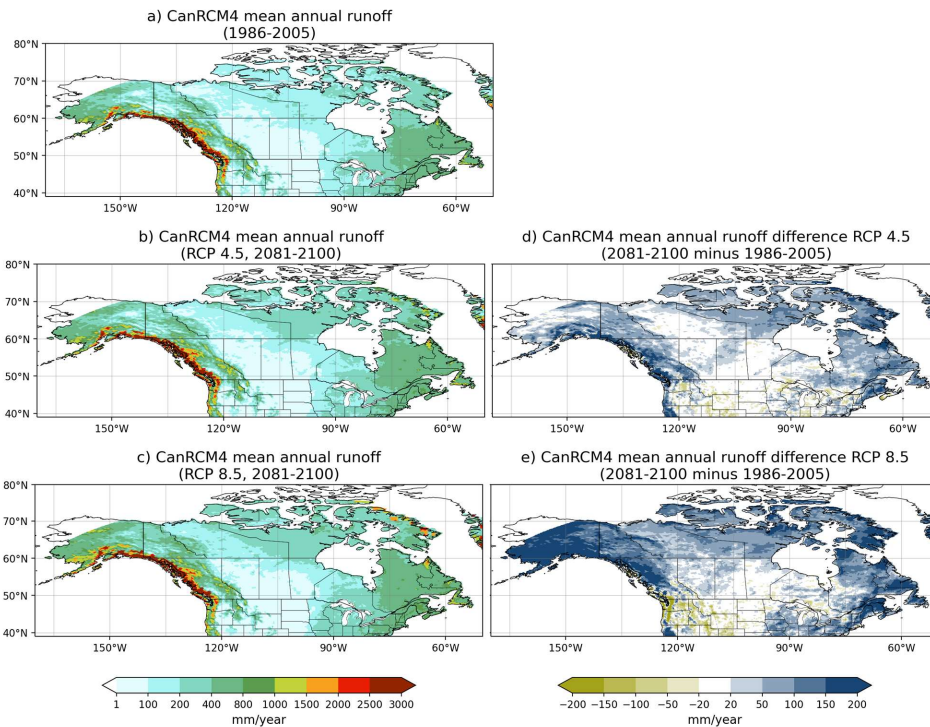
Deleted: then

Deleted:



683 **Figure 6:** Comparison of CanRCM4 simulated temperature for the 1986-2005 period and for the
684 2081-2100 periods, for RCP 4.5 and 8.5 scenarios.

Deleted: ¶

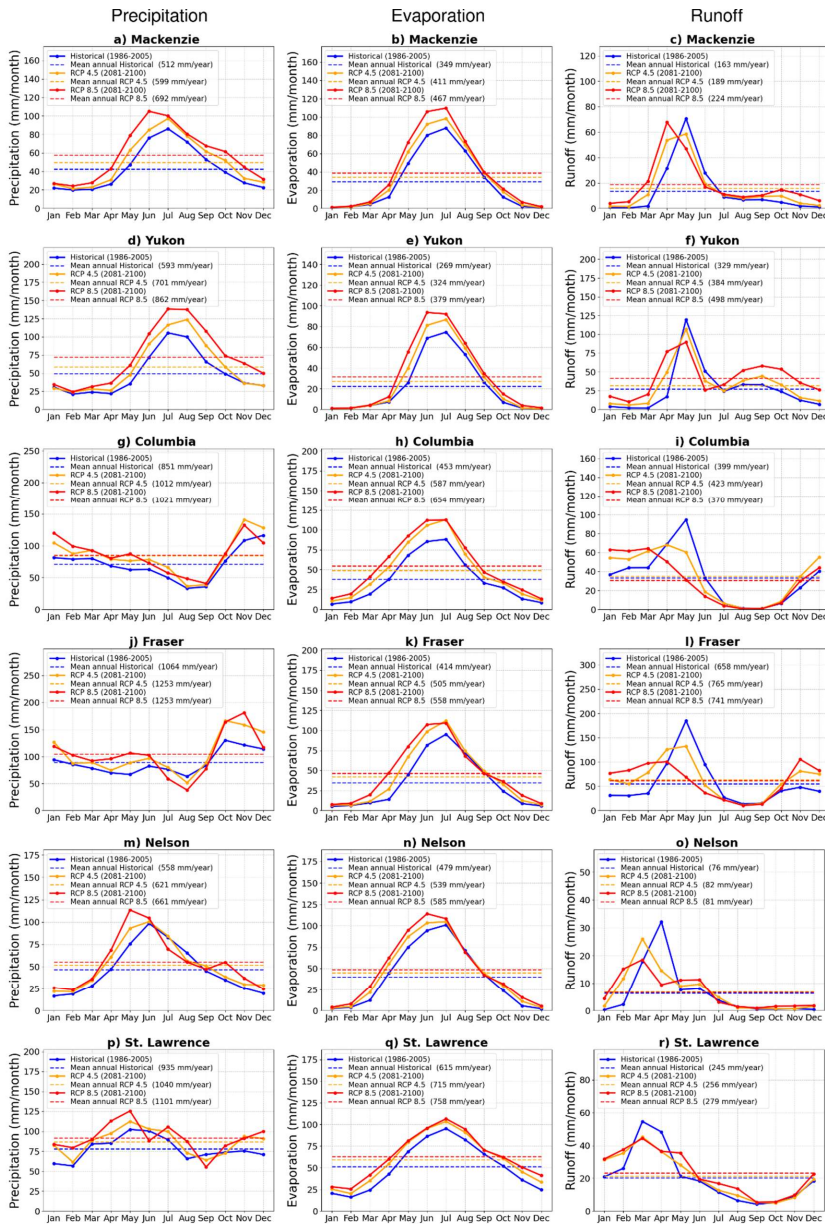


687

688 **Figure 7:** Comparison of CanRCM4 simulated runoff for the 1986-2005 period and for the 2081-
 689 2100 periods, for RCP 4.5 and 8.5 scenarios.

690

691 In Figure 7 runoff increases generally everywhere in Canada for the RCP 4.5 and RCP 8.5 scenarios
 692 with larger changes on the west and east coasts, and in northern Canada, following a similar
 693 pattern of changes in precipitation. Runoff reduces in parts of the southern Columbia River basin
 694 in the United States in the RCP 4.5 scenario, and these decreases become more pronounced and
 695 widespread over the north-western Pacific region in the RCP 8.5 scenario including the Fraser
 696 River basin in Canada.



697
698
699
700
701
702
703
704
705
706
707
708
709
710
711
712
713
714
715
716
717
718
719
720
721
722
723
724
725
726

Figure 8: Comparison of the annual cycle of basin-wide averaged CanRCM4 simulated water budget components for each river basin for the historical (1986-2005) period and the two future scenarios RCP 4.5 and 8.5 (2081-2100): precipitation (left column), evaporation (middle column), and runoff (right column).

731

732

733

734

735

736

737

738

739

740

741

742

743

744

745

746

747

748

749

750

751

752

753

754

755

756

757

758

759

760

761

762

763

764

765

766

767

768

769

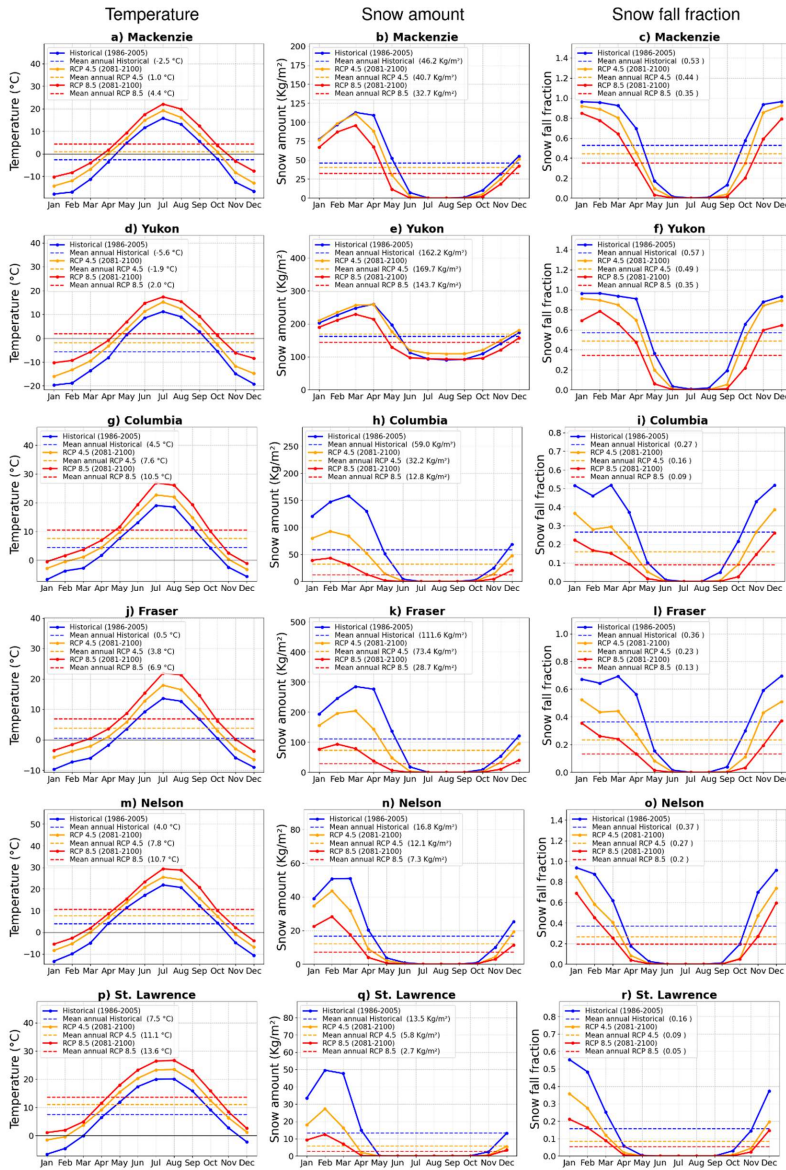


Figure 9: Comparison of the annual cycle of basin-wide averaged CanRCM4 simulated temperature (left column), snow water equivalent amount (middle column), and snowfall fraction (right column) for the historical (1986-2005) period and the two future scenarios RCP 4.5 and 8.5 (2081-2100).

774 Figure 8 shows the annual cycle of the simulated water budget components
 775 (precipitation, evaporation, and runoff) for the six river basins considered in this study for the
 776 historical (1986-2005) period and the two future scenarios, RCP 4.5 and 8.5 (2081-2100). As in
 777 Figure 4, the mean annual values are shown as dashed lines, and their magnitude is noted in the
 778 legend.

Deleted: lines

779 **Table 2:** Evaporation and runoff ratios for the six river basins simulated by CanRCM4 for the
 780 historical period (1986-2005) and the two future scenarios (RCP 4.5 and 8.5, 2081-2100). The
 781 evaporation (runoff) ratio is the ratio of mean annual evaporation (runoff) to precipitation.
 782

Deleted: five

River basin	Evaporation ratio (E/P)			Runoff ratio (R/P)		
	Historical (1986-2005)	RCP 4.5 (2081-2100)	RCP 8.5 (2081-2100)	Historical (1986-2005)	RCP 4.5 (2081-2100)	RCP 8.5 (2081-2100)
Mackenzie	0.682	0.686	0.675	0.318	0.316	0.324
Yukon	0.454	0.462	0.440	0.555	0.548	0.579
Columbia	0.532	0.580	0.641	0.469	0.418	0.362
Fraser	0.389	0.403	0.445	0.618	0.611	0.591
Nelson	0.858	0.868	0.885	0.136	0.132	0.123
St. Lawrence	0.664	0.686	0.684	0.314	0.294	0.302

783
 784 The evaporation (E/P) and runoff (R/P) ratios for the six river basins for the historical period and
 785 the two future scenarios are shown in Table 2 and allow to see how the partitioning of
 786 precipitation into evaporation and runoff changes with climate. For the mean annual values of P,
 787 E, and R reported in Figure 8, P is balanced to within 1% by E+R for all river basins (except the St.
 788 Lawrence) and all scenarios, except for the Yukon (for RCP 8.5) and the Fraser River basins (for
 789 RCP 4.5 and 8.5) for which (E+R) is higher than P indicating that ΔS is not zero (see equation 1).
 790 As a result, (E/P) and (R/P) also add to one for all river basins except for the Yukon (RCP
 791 8.5, $(E + R)/P = 1.02$) and the Fraser River (RCP 4.5, $(E + R)/P = 1.014$, and RCP 8.5,
 792 $(E + R)/P = 1.036$) basins. For the St. Lawrence River basin, the imbalance is around 2%
 793 because of the presence of the Great Lakes which had to be excluded from the river basin mask.

Deleted: (

Deleted:)

798 Since basin-wide averaged calculations are done at 0.5° latitude-longitude resolution, and the
799 actual domain of CanRCM4 is on a rotated latitude-longitude projection this led to slightly more
800 rounding errors for the St. Lawrence than other river basins.

801 For all river basins considered, precipitation increases for both future scenarios with the
802 increase being larger for the RCP 8.5 scenario consistent with Figures 5d and 5e. The response of
803 evaporation to changes in climate is expected. The increase in precipitation and temperature
804 yields an increase in evaporation for future scenarios for all river basins. Simulated runoff does
805 not increase as much as precipitation since evaporation also increases. The runoff ratio, in Table
806 2, increases for the northerly Mackenzie and the Yukon River basins while it decreases for the
807 southerly Nelson, St. Lawrence, and especially for the Fraser and Columbia River basins which
808 are characterized by milder climate owing to their location in the Pacific north-western region.
809 This is because the increase in precipitation is more than enough to compensate for the increase
810 in evaporation (associated with a warmer climate) for the northern river basins but not for the
811 southern ones (as seen earlier in Figure 7 where runoff begins to decrease in parts of the
812 Columbia and Fraser River basins). The absolute runoff amount in Figure 8 increases for the
813 Mackenzie and Yukon River basins, in the RCP 4.5 and 8.5 scenarios compared to the historical
814 simulation, but doesn't change much for the Columbia, Fraser, Nelson, and St. Lawrence River
815 basins. However, the seasonality of runoff changes for all river basins, and the peak in simulated
816 runoff either occurs earlier in the year, occurs with reduced magnitude, or both. Canadian rivers
817 are dominated by spring snowmelt and this runoff behaviour is associated with snow melt
818 occurring earlier in the year in the RCP 4.5 scenario than in the historical simulation, and occurring
819 even earlier in the RCP 8.5. This is seen in Figure 9 which shows the simulated annual cycle of

Deleted:

Deleted: peak

Deleted: ,

Deleted: scenario than in the RCP 4.5 scenario

824 temperature changes, snow amount, and snowfall as a fraction of total precipitation for the
825 historical period and the two RCP scenarios for the six river basins. In Figure 9 the mean annual
826 temperature increases from the historical period to the RCP 4.5 scenario, and from the RCP 4.5
827 to RCP 8.5 scenario, are between 3 and 3.5 °C for the six river basins considered here. The middle
828 column of Figure 9 shows that in addition to earlier snowmelt the amount of snow in the winter
829 months decreases for all river basins with climate warming. The only exception to this is the
830 Yukon River basin in which the mean annual snow amount increases marginally in the RCP 4.5
831 scenario (Figure 9e). As expected, the fraction of precipitation falling as snow also decreases with
832 climate warming for all river basins (right column, Figure 9).

833

Deleted: is

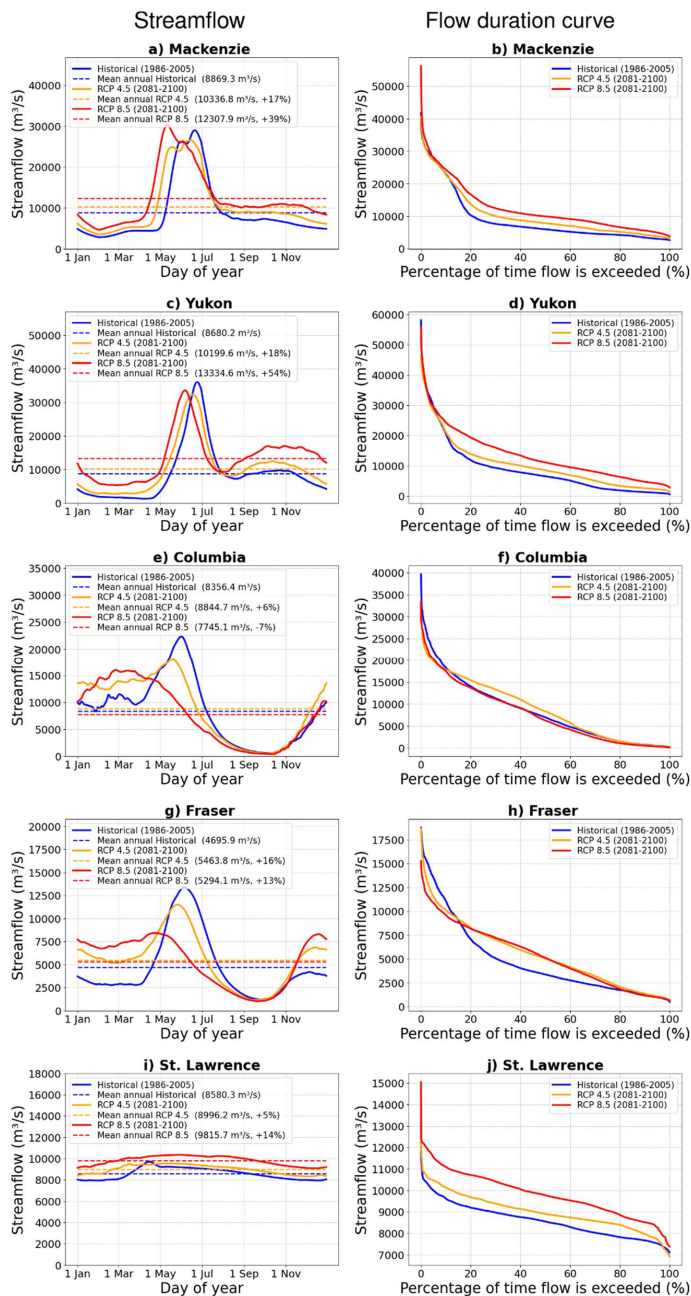


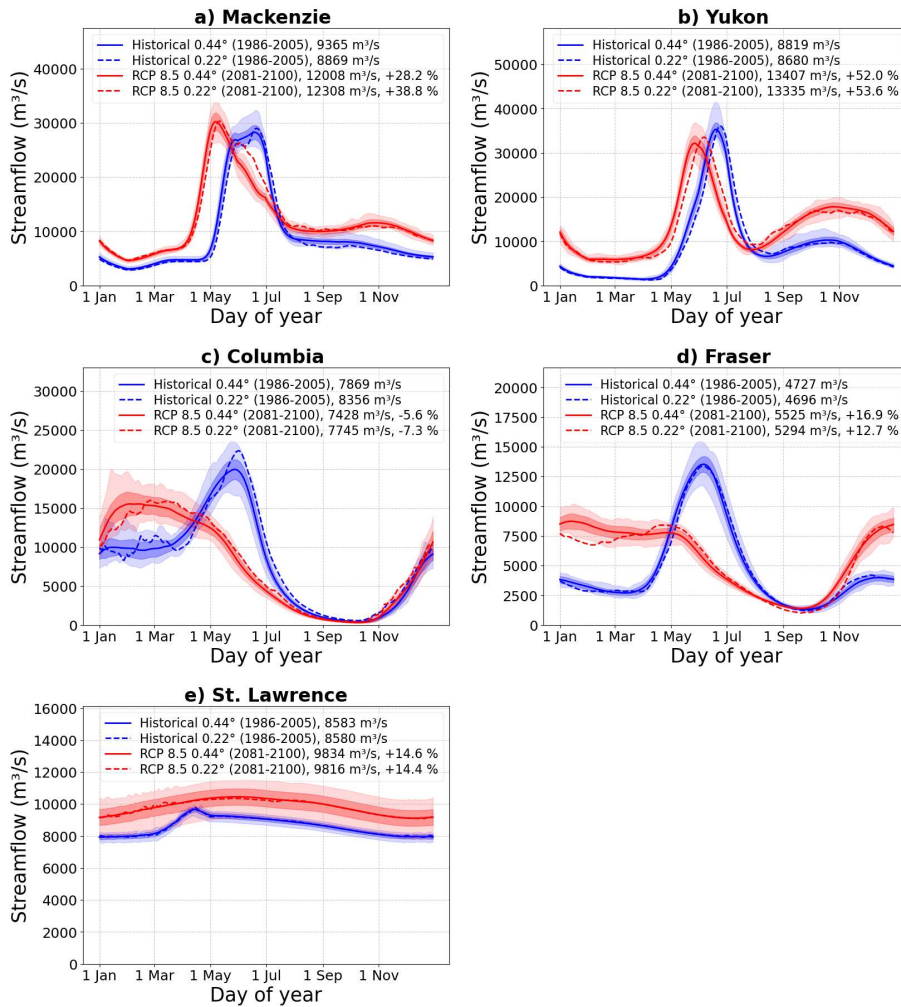
Figure 10: Comparison of the simulated daily streamflow (left column) and flow duration curves (right column) for the historical (1986-2005) period and the two future scenarios RCP 4.5 and 8.5 (2081-2100) for the river basins considered. The Nelson River is excluded for which we only evaluated annual streamflow values that are mentioned in the text.

Deleted: monthly

Deleted: here because

Deleted: its

Deleted: which



865 **Figure 11:** Comparison of the simulated daily streamflow for the historical (1986-2005) period
 866 and the RCP 8.5 scenario (2081-2100) for the river basins considered in this study from the
 867 0.22° and 0.44° simulations. The results from the 0.22° simulations (shown earlier in Figure 10)
 868 are shown as dashed lines. The uncertainty range for the 0.44° simulations is based on results
 869 from CanRCM4's 50-member large ensemble. The solid lines indicate the mean across 50
 870 members the light shading indicates the full range, and the dark shading indicates the mean \pm
 871 one standard deviation range, for the 0.44° simulations. [The Nelson River is excluded for which](#)

Deleted: monthly

873 [only annual streamflow values are analyzed.](#)

874

875 Figure 10 compares simulated [daily streamflow](#) and flow duration curves [averaged over](#)

876 the historical (1986-2005) period with those [averaged over](#) the two future scenarios RCP 4.5 and

877 8.5 (2081-2100) for the [river basins considered here excluding the Nelson River](#). The flow

878 duration curves are calculated using daily streamflow values. [The legends in Figure 10 for the](#)

879 streamflow figures in the left column show mean annual values but also the change from the

880 simulated historical values for the RCP 4.5 and 8.5 scenarios. The mean annual streamflow

881 increases for all rivers for both the RCP 4.5 and 8.5 scenarios, except for the Columbia River for

882 the RCP 8.5 scenario (-7%). The increase in simulated annual streamflow is largest for the

883 Mackenzie (+16%, +39%) and Yukon Rivers (+17%, +53%) for the RCP 4.5 and 8.5 scenarios, due

884 to higher precipitation increase in these two basins (Figure 8). The increase in annual streamflow

885 for other rivers is smaller and between 6% and 14%. [Daily streamflow and flow duration curves](#)

886 [are not shown for the Nelson River because we do not consider anthropogenic flow regulation,](#)

887 [as mentioned earlier. The simulated mean annual streamflow for the Nelson River increases from](#)

888 [2556.6 m³/s \(for the 1986-2005 period\) to 2774.8 and 2723.8 m³/s for the RCP 4.5 \(+9%\) and 8.5](#)

889 [\(+7%\) scenarios, respectively \(for the period 2081-2100\).](#)

890 The changes in streamflow seasonality are larger for the southerly Columbia and Fraser

891 Rivers than for the northerly Mackenzie and Yukon Rivers. The peak [daily streamflow](#) for the

892 Yukon River still occurs in June given it's the coldest river basin (Figure 4d) and the streamflow

893 seasonality is still dominated by the spring snowmelt. [The simulated daily peak streamflow for](#)

894 [the Yukon River occurs on 24 June for the historical period \(1986-2005\), and 18 June and 6 June,](#)

Deleted: z

Deleted: monthly

Deleted: for

Deleted: from

Deleted: six

Deleted: Monthly

Deleted: Daily streamflow and flow duration curves are not shown for the Nelson River because we do not consider anthropogenic flow regulation, as mentioned earlier. The simulated mean annual streamflow for the Nelson River increases from 2556.6 m³/s (for the 1986-2005 period) to 2774.8 and 2723.8 m³/s for the RCP 4.5 and 8.5 scenarios, respectively (for the period 2081-2100).

Deleted: monthly

Deleted: 1

910 respectively, for RCP 4.5 and 8.5 scenarios for the period 2081-2100. Streamflow for the Yukon
 911 River also begins to increase earlier due to earlier snowmelt (Figure 9e). While the spring peak
 912 streamflow reduces in both RCP 4.5 and 8.5 scenario during the month of June and part of July,
 913 streamflow increases for most other months for the Yukon River. The Mackenzie River shows
 914 similar behaviour to the Yukon River in terms of earlier shifts of spring streamflow peaks with
 915 climate warming but the spring peak is higher for the RCP 8.5 scenario. The mean simulated daily
 916 peak streamflow for the Mackenzie River occurs on 21 June for the historical period (1986-2005),
 917 and 14 June and 11 May, respectively, for RCP 4.5 and 8.5 scenarios for the period 2081-2100.
 918 Similar to Yukon, although the streamflow is lower for the Mackenzie River during the month of
 919 June and part of the July, it increases for most other months. The corresponding changes in
 920 streamflow are also seen in the flow duration curves. For these two rivers the frequency of the
 921 occurrence of flows that occur greater than about 5% of the time in the historical simulation
 922 increases in the future. The Columbia and the Fraser Rivers experience much larger changes in
 923 their seasonality as their primarily snow-dominated flow regimes change to more hybrid flow
 924 regimes. The snowmelt-driven streamflow peak in spring is reduced considerably for future
 925 scenarios since a lower fraction of fall, winter, and spring precipitation falls as snow. As a result,
 926 streamflow increases from October to April since precipitation falling as rain, as opposed to snow,
 927 yields runoff that runs straight into the rivers. Additionally, the large reduction in snowpack
 928 volume together with earlier melt (Figure 9k and 9h) affects the seasonality of the Fraser and
 929 Columbia Rivers streamflow and causes pronounced shifts in peak flows. The mean simulated
 930 daily peak streamflow for the Columbia River occurs on 1 June for the historical period (1986-
 931 2005), and 19 May and 25 February, respectively, for RCP 4.5 and 8.5 scenario for the period

Deleted: However, despite the peak streamflow still occurring in June the s...

Deleted: does

Deleted: June streamflow peak doesn't change substantially

Deleted: For t

Deleted: ,

Deleted: occurring

Deleted: the peak streamflow occurs in June in the RCP 4.5 scenario as in the historical simulation but a month earlier in the RCP 8.5 scenario.

Deleted: Like

Deleted: the

Deleted: peak

Deleted: doesn't change substantially

Deleted: se

Deleted: which show that f

Deleted: nival

Deleted: s

950 [2081-2100. For the Fraser River, the mean simulated peak streamflow, occurs on 5 June for the](#)
951 [historical period \(1986-2005\), and 26 May and 21 April, respectively, for RCP 4.5 and 8.5 scenario](#)
952 [for the period 2081-2100.](#) The pronounced changes in the Fraser River basin peak flow are
953 apparent in its flow duration curve (Figure 10h) which shows a decrease (increase) in the
954 frequency of streamflow events which occurred less (more) than about 16% of the time and
955 result in a more equitable streamflow regime with a pronounced reduction in its seasonality.
956 Simulated streamflow for the St. Lawrence River shows very little seasonality and since annual
957 streamflow increases for both scenarios, the flow duration curve simply moves up (Figure 10j).

Deleted: m

958 3.3 Uncertainty in simulated changes in future streamflow

959 [Using the large ensemble simulations that are](#) available for the historical [period](#) and the
960 RCP 8.5 scenario [at 0.44 ° resolution, we](#) quantified the uncertainty [in the simulated streamflow](#),
961 associated with the internal variability of the CanRCM4 model. [Similar to the 0.22° resolution,](#)
962 [we regridded the 0.44° runoff at CanRCM4's rotated latitude longitude projection to 0.5° regular](#)
963 [latitude longitude projection for use as input into the river routing scheme.](#) This is illustrated in
964 Figure 11 which shows the simulated [daily](#) streamflow for all the rivers considered here except
965 the Nelson River. In Figure 11, the solid lines show the average across the 50 members of the
966 [large ensemble](#), light shading shows the full range of the results, and dark shading shows the
967 mean ± one standard deviation range (this implies the [16%-84%, i.e. 68%](#) range when assuming
968 normally distributed monthly streamflow values). In addition, streamflow from the 0.22°
969 simulations (from Figure 10) is shown as dashed lines to allow direct comparison of results from
970 the 0.22° and 0.44° simulations.

Deleted: In addition to the 0.22° simulations for the North American domain, simulation results are also available from the 50-member large ensemble (LE) of CanRCM4 at 0.44° resolution. ...

Deleted: T

Deleted: LE

Deleted: data

Deleted: are,

Deleted: however, only

Deleted: simulation

Deleted: . Similar to the 0.22° resolution, we regridded the 0.44° runoff at CanRCM4's rotated latitude longitude projection to 0.5° regular latitude longitude projection for use as input into the river routing scheme. The use of the results from the LE...allows us to allows us to

Deleted: allows us to

Deleted: y

Deleted: associated with

Deleted: based on the spread in the simulated results

Deleted: LE

Deleted: 5

Deleted: 95

Deleted: (

Deleted:)

997 The changes in simulated streamflow are consistent between the 0.22° and 0.44°
998 simulations. ~~The results from the 0.44° simulations are also notably smoother compared to the~~
999 ~~0.22° simulations since the 0.44° results are also averaged over the 50 ensemble members in~~
1000 ~~addition to the 20-year time period.~~ For the most part, the results from the 0.22° simulations lie
1001 within the full range of results from the 0.44° simulations.
1002 This is expected since the driving climate at the boundaries of CanRCM4 based on CanESM2 is
1003 the same in both resolutions. The magnitude of change from the historical to the RCP 8.5 scenario
1004 (see legend for individual rivers) are, however, somewhat different. This is also expected because
1005 ~~the coarser resolution 0.44° simulations is less representative of the basin topography than the~~
1006 ~~0.22° simulations.~~ The day of peak streamflow occurs a few days early in 0.22° simulations than
1007 in the 0.44° simulations for the Mackenzie and Yukon Rivers. Overall, the large ensemble from
1008 the 0.44° simulations helps to provide context for results from the 0.22° simulations.

1009 Overall, despite the differences in the magnitude of changes, the direction and variability
1010 of change obtained from this study is generally consistent with the previous studies using basin-
1011 scale hydrologic models, driven by statistically downscaled and bias-corrected climate model
1012 data, for instance for the Fraser River (Islam et al., 2019; Shrestha et al., 2012), the Columbia
1013 River (Schnorbus et al., 2014) and the Yukon River (Hay and McCabe, 2010). The results presented
1014 here are also comparable to the projections from global and regional scale hydrologic models,
1015 e.g. for the Mackenzie River basin (Krysanova et al., 2017, 2020).

1017 4. Summary and conclusions

Deleted: than the result from

Deleted: in addition to the 20-year time period

Deleted: ,

Deleted: and f

Deleted: ,

Deleted: The results from the 0.44° simulations are notably smoother...

Deleted: exact values and the

Deleted: since these simulations are different from the 0.22° simulations. T

Deleted: of the

Deleted: implies that the

Deleted: is not as realistically represented as in

Deleted: In particular, for the Yukon, the results based on the 0.22° simulation indicate that the month and the magnitude of peak streamflow do not change significantly in the RCP 8.5 scenario (Figure 10c), while those based on 0.44° suggest that they do

Deleted: There are some differences between 0.22° and 0.44° results for the Mackenzie and Fraser Rivers too.

Deleted: LE

Formatted: French (Canada)

Formatted: English (Canada)

Formatted: English (Canada)

1039 This study offers a consistent analysis of results across six river basins in Canada based on
1040 results from the CanRCM4 model. Despite the biases in simulated present-day CanRCM4 climate,
1041 and some differences in the results based on 0.22° and 0.44° simulations, the results provide
1042 useful information about changes in simulated streamflow that is consistent with expectations
1043 of process behaviour in a warmer climate, and with published studies.

Deleted: η

Deleted: although

Deleted: a single climate model

1044 Neither future precipitation nor temperature changes are uniform across Canada.
1045 Simulated precipitation increases are higher closer to the west and east coasts, and simulated
1046 temperature changes are higher towards the Arctic. Similar to precipitation, runoff changes are
1047 also higher closer to the west and east coasts. The changes in simulated streamflow indicate how
1048 the present-day climate state of river basins plays a role in their response to climate change. The
1049 results yield two broadly distinct responses of monthly streamflow changes to climate warming,
1050 up until the end of this century, for the northerly Mackenzie and Yukon rivers and the southerly
1051 Fraser and Columbia rivers. Despite higher future projected temperature changes in Canada's
1052 north, peak streamflow for the Mackenzie and Yukon rivers is still dominated by the spring
1053 snowmelt. This is because the present-day colder states of these river basins imply that even
1054 after around 6-7 °C warming, the basin-wide average temperatures are cold enough to not
1055 sufficiently change their snowmelt-dominated streamflow regimes. Changes, however, do occur
1056 in streamflow seasonality for these two rivers. Mean peak daily streamflow occurs earlier by
1057 about 6-7 days for the Mackenzie and Yukon Rivers in the RCP 4.5 scenario and about 28 days for
1058 the Mackenzie River and 12 days for the Yukon River for the RCP 8.5 scenario (Figure 10). Earlier
1059 start of the snowmelt is the primary factor for the changes in peak streamflow and its time of
1060 occurrence, while the streamflow increases during the rest of the year, (except for June and part

Deleted: literature

Deleted: P

Deleted: streamflow month changes

Deleted: from June to May

Deleted: 8

Deleted: for both 0.22°

Deleted: 9

Deleted: a

Deleted: and 0.44° (Figure 11a) simulations and for the Yukon River in the RCP 8.5 scenario for 0.44° simulations (Figure 11b)...

Deleted: Other than the

Deleted: month and peak

Deleted: occurrence

Deleted: snowmelt occurs earlier so streamflow starts increasing earlier in the spring

Deleted: and

Deleted: also increases

1082 of July) are driven by increase in precipitation. Additionally, a higher fraction of winter
1083 precipitation occurring as rainfall drives the winter streamflow increases. In contrast, the
1084 streamflow seasonality for the southerly Fraser and Columbia rivers is significantly more affected
1085 by warmer temperatures because the mean annual basin-wide temperature for these river basins
1086 is already above 0° C for the historical period. Both these rivers experience pronounced changes
1087 in their streamflow seasonality. The peak daily streamflow for both rivers decreases considerably
1088 and occurs about 45 days earlier for the Fraser River and about 100 days earlier for the Columbia
1089 River in the RCP 8.5 scenario. These results compare reasonably to the 1-2 months earlier peak
1090 in previous studies for the Fraser River (Islam et al., 2019; Shrestha et al., 2012) but are higher
1091 than the two month earlier peak for the Columbia River (Schnorbus et al., 2014) that used results
1092 from multiple climate models. Shrestha et al. (2021a) used CanRCM4 data to evaluate snowpack
1093 response to varying degrees of warming. They found that snowpack reduction using CanRCM4-
1094 LE is higher than the ensemble of results obtained by driving a hydrological model with data from
1095 other climate models (their supplementary information), consistent with CanESM2's higher
1096 climate sensitivity. For the Nelson and the St. Lawrence Rivers which show very little seasonality
1097 the effect of climate change is reflected in the changes in mean annual streamflow.

1098 The results presented here also appear to show that the simulated changes in streamflow
1099 are somewhat resolution-dependent. This would be expected especially for topography-
1100 dominated river basins. If a large ensemble of 50 members for the 0.22° resolution was also
1101 available, it would have been easier to draw firm conclusions about the effect of the spatial
1102 resolution on changes in simulated streamflow.

Deleted: due

Deleted: primarily

Deleted: to an

Deleted: two

Deleted: months

Deleted: 2-3

Deleted: months

Deleted: appear exaggerated

Deleted: d

Deleted: and

Deleted: rivers

Deleted: LE

1115 There are two primary limitations of the work presented here. First, we use results from
1116 only one climate model. It would have been ideal to use runoff from other regional climate
1117 models to provide an uncertainty range based on the spread across different climate models.
1118 This would have also allowed ed us to evaluate how the spread across v models compares to the
1119 spread across the 50 members of the CanRCM4 large ensemble. Second, the results are based on
1120 direct output from the CanRCM4 climate model and direct climate model output is biased. This
1121 limitation is tied to our methodology. The use of bias-corrected climate data v inevitably implies
1122 using a different hydrological model or land surface scheme, than the land surface component of
1123 CanRCM4, and forcing it with bias-corrected climate data to obtain runoff. Finally, there are
1124 uncertainties associated with the routing process itself. As mentioned earlier, the routing scheme
1125 accounts for ice jams in a simplified manner and anthropogenic flow regulation is not taken into
1126 account. The implicit assumption when using raw climate model output is that, despite the biases
1127 in simulated climate, it is possible to derive useful information about the impact of climate
1128 change on the simulated streamflow and other components of the hydrological budget. The
1129 Canada-wide results presented here have allowed us to differentiate between the hydrological
1130 response of northerly Mackenzie and Yukon Rivers, and the southerly Fraser and Columbia Rivers,
1131 to climate change in a consistent manner. Furthermore, our results help fill the gaps in regions
1132 across Canada, where no climate model driven hydrological projections are available. Within the
1133 scope of this study, we have only evaluated streamflow at the mouth of the six major rivers
1134 considered here. The full data set of daily simulated streamflow for the 20-year historical (1986-
1135 2005) and future periods (2081-2100) for the two scenarios, based on runoff from the 0.22°
1136 simulations, is made available as detailed in the data availability section.

Deleted: the

Deleted: LE

Deleted: B

Deleted: ing

Deleted: in our case

Deleted: Finally, there are uncertainties associated with the routing process itself. As mentioned earlier, the routing scheme accounts for ice jams in a simplified manner and anthropogenic flow regulation is not taken into account.

1146 Large ensembles are now becoming more common. The challenge for similar future
1147 studies is to consider the inter-model and intra-model (based on ensemble members of the same
1148 model) spreads in a same framework to derive an uncertainty estimate that ~~takes into account~~
1149 both types of uncertainties.

Deleted: the

Deleted: is consistent

Deleted: with

1150
1151

1152 Acknowledgment

1153

1154 We thank Daniel Peters for the helpful discussions at the beginning of this work and Sal Curasi
1155 and Gesa Meyer for providing comments on the final version of this manuscript. We also
1156 acknowledge the efforts of the climate modelling team at the Canadian Centre for Climate
1157 Modelling and Analysis (CCCma) who made the results from CanRCM4 available. We also thank
1158 the two anonymous reviewers who provide useful comments and helped us address the
1159 questions related to model bias and the differences in land surface and hydrological models.
1160 Finally, we would like to thank our handling editor (Alexander Gruber) for taking on our
1161 manuscript and giving us the opportunity to revise our manuscript.

Deleted:

1162

1163 Data availability

1164

1165 The CanRCM4 data from 0.22° simulations used in this study are available from CCCma website
1166 (<https://climate-modelling.canada.ca/climatemodeldata/canrcm/CanRCM4/>). The data from
1167 the 0.44° CanRCM4 large ensemble are available from Environment and Climate Change
1168 Canada (<https://open.canada.ca/data/en/dataset/83aa1b18-6616-405e-9bce-af7ef8c2031c>).

Deleted: Code/

1169

1170 NetCDF files of simulated daily streamflow from the historical (1986-2005) and the two future
1171 scenarios (RCP 4.5 and 8.5, 2081-2100) at 0.5° resolution are available on Zenodo for the entire
1172 North American domain of CanRCM4 (doi:10.5281/zenodo.12775139). These streamflow data
1173 correspond to the runoff from the 0.22° simulations.

Formatted: Font: Not Bold

1174

1175 Author contributions

1176

1177 VKA designed the study and wrote the majority of the manuscript. AL implemented river
1178 routing to operate at 0.5° resolution and performed all the simulations. RS and AL contributed
1179 to the manuscript text. RS also performed a literature review of existing studies that focus on
1180 the impact of climate change on Canadian rivers.

1186

1187 **Competing interests**

1188

1189 The authors declare that they have no competing interests.

1190

1191 **References**

1192 Alaya, M. A. B., Zwiers, F., and Zhang, X.: Evaluation and Comparison of CanRCM4 and CRCM5 to
1193 Estimate Probable Maximum Precipitation over North America, *J. Hydrometeorol.*, 20, 2069–2089,
1194 <https://doi.org/10.1175/JHM-D-18-0233.1>, 2019.

1195 Arora, V., Seglenieks, F., Kouwen, N., and Soulis, E.: Scaling aspects of river flow routing, *Hydrol.*
1196 *Process.*, 15, 461–477, <https://doi.org/10.1002/hyp.161>, 2001.

1197 Arora, V. K. and Boer, G. J.: Effects of simulated climate change on the hydrology of major river basins, *J.*
1198 *Geophys. Res. Atmospheres*, 106, 3335–3348, <https://doi.org/10.1029/2000JD900620>, 2001.

1199 Arora, V. K. and Boer, G. J.: A Representation of Variable Root Distribution in Dynamic Vegetation
1200 Models, *Earth Interact.*, 7, 1–19, [https://doi.org/10.1175/1087-3562\(2003\)007<0001:AROVRD>2.0.CO;2](https://doi.org/10.1175/1087-3562(2003)007<0001:AROVRD>2.0.CO;2),
1201 2003.

1202 Arora, V. K. and Boer, G. J.: A parameterization of leaf phenology for the terrestrial ecosystem
1203 component of climate models, *Glob. Change Biol.*, 11, 39–59, [https://doi.org/10.1111/j.1365-](https://doi.org/10.1111/j.1365-2486.2004.00890.x)
1204 [2486.2004.00890.x](https://doi.org/10.1111/j.1365-2486.2004.00890.x), 2005.

1205 Arora, V. K. and Boer, George. J.: A variable velocity flow routing algorithm for GCMs, *J. Geophys. Res.*
1206 *Atmospheres*, 104, 30965–30979, <https://doi.org/10.1029/1999JD900905>, 1999.

1207 Arora, V. K. and Harrison, S.: Upscaling river networks for use in climate models, *Geophys. Res. Lett.*, 34,
1208 <https://doi.org/10.1029/2007GL031865>, 2007.

1209 Arora, V. K., Boer, G. J., Christian, J. R., Curry, C. L., Denman, K. L., Zahariev, K., Flato, G. M., Scinocca, J.
1210 F., Merryfield, W. J., and Lee, W. G.: The Effect of Terrestrial Photosynthesis Down Regulation on the
1211 Twentieth-Century Carbon Budget Simulated with the CCCma Earth System Model, *J. Clim.*, 22, 6066–
1212 6088, <https://doi.org/10.1175/2009JCLI3037.1>, 2009.

1213 Arora, V. K., Scinocca, J. F., Boer, G. J., Christian, J. R., Denman, K. L., Flato, G. M., Kharin, V. V., Lee, W.
1214 G., and Merryfield, W. J.: Carbon emission limits required to satisfy future representative concentration
1215 pathways of greenhouse gases, *Geophys. Res. Lett.*, 38, n/a-n/a,
1216 <https://doi.org/10.1029/2010GL046270>, 2011.

1217 Beltaos, S.: Advances in river ice hydrology, *Hydrol. Process.*, 14, 1613–1625,
1218 [https://doi.org/10.1002/1099-1085\(20000630\)14:9<1613::AID-HYP73>3.0.CO;2-V](https://doi.org/10.1002/1099-1085(20000630)14:9<1613::AID-HYP73>3.0.CO;2-V), 2000.

1219 Bonsal, B., Shrestha, R. R., Dibike, Y., Peters, D. L., Spence, C., Mudryk, L., and Yang, D.: Western
1220 Canadian Freshwater Availability: Current and Future Vulnerabilities, *Environ. Rev.*, 28, 528–545,
1221 <https://doi.org/10.1139/er-2020-0040>, 2020.

1222 Budhathoki, S., Rokaya, P., and Lindenschmidt, K.-E.: Impacts of future climate on the hydrology of a
1223 transboundary river basin in northeastern North America, *J. Hydrol.*, 605, 127317,
1224 <https://doi.org/10.1016/j.jhydrol.2021.127317>, 2022.

1225 Chegwiddden, O. S., Nijssen, B., Rupp, D. E., Arnold, J. R., Clark, M. P., Hamman, J. J., Kao, S.-C., Mao, Y.,
1226 Mizukami, N., Mote, P. W., Pan, M., Pytlak, E., and Xiao, M.: How Do Modeling Decisions Affect the
1227 Spread Among Hydrologic Climate Change Projections? Exploring a Large Ensemble of Simulations
1228 Across a Diversity of Hydroclimates, *Earths Future*, 7, 623–637, <https://doi.org/10.1029/2018EF001047>,
1229 2019.

1230 Chen, Y. and She, Y.: Long-term variations of river ice breakup timing across Canada and its response to
1231 climate change, *Cold Reg. Sci. Technol.*, 176, 103091,
1232 <https://doi.org/10.1016/j.coldregions.2020.103091>, 2020.

1233 Côté, J., Gravel, S., Méthot, A., Patoine, A., Roch, M., and Staniforth, A.: The Operational CMC–MRB
1234 Global Environmental Multiscale (GEM) Model. Part I: Design Considerations and Formulation, *Mon.*
1235 *Weather Rev.*, 126, 1373–1395, [https://doi.org/10.1175/1520-0493\(1998\)126<1373:TOCMGE>2.0.CO;2](https://doi.org/10.1175/1520-0493(1998)126<1373:TOCMGE>2.0.CO;2),
1236 1998.

1237 Deser, C., Lehner, F., Rodgers, K. B., Ault, T., Delworth, T. L., DiNezio, P. N., Fiore, A., Frankignoul, C.,
1238 Fyfe, J. C., Horton, D. E., Kay, J. E., Knutti, R., Lovenduski, N. S., Marotzke, J., McKinnon, K. A., Minobe, S.,
1239 Randerson, J., Screen, J. A., Simpson, I. R., and Ting, M.: Insights from Earth system model initial-
1240 condition large ensembles and future prospects, *Nat. Clim. Change*, 10, 277–286,
1241 <https://doi.org/10.1038/s41558-020-0731-2>, 2020.

1242 Dibike, Y., Muhammad, A., Shrestha, R. R., Spence, C., Bonsal, B., de Rham, L., Rowley, J., Evenson, G.,
1243 and Stadnyk, T.: Application of dynamic contributing area for modelling the hydrologic response of the
1244 Assiniboine River basin to a changing climate, *J. Gt. Lakes Res.*, 47, 663–676,
1245 <https://doi.org/10.1016/j.jglr.2020.10.010>, 2021.

1246 ECCC: The Canadian Regional Climate Model Large Ensemble. Environment and Climate Change Canada
1247 (ECCC), Government of Canada Open Data Portal. Available at:
1248 <https://open.canada.ca/data/en/dataset/83aa1b18-6616-405e-9bce-af7ef8c2031c>, Gatineau, QC,
1249 Canada, 2018.

1250 Gosling, S. N., Taylor, R. G., Arnell, N. W., and Todd, M. C.: A comparative analysis of projected impacts
1251 of climate change on river runoff from global and catchment-scale hydrological models, *Hydrol. Earth*
1252 *Syst. Sci.*, 15, 279–294, <https://doi.org/10.5194/hess-15-279-2011>, 2011.

1253 Harris, I., Osborn, T. J., Jones, P., and Lister, D.: Version 4 of the CRU TS monthly high-resolution gridded
1254 multivariate climate dataset, *Sci. Data*, 7, 109, <https://doi.org/10.1038/s41597-020-0453-3>, 2020.

1255 Hattermann, F. F., Vetter, T., Breuer, L., Su, B., Daggupati, P., Donnelly, C., Fekete, B., Flörke, F., Gosling,
1256 S. N., P Hoffmann, Liersch, S., Masaki, Y., Motovilov, Y., Müller, C., Samaniego, L., Stacke, T., Wada, Y.,
1257 Yang, T., and Krysaova, V.: Sources of uncertainty in hydrological climate impact assessment: a cross-
1258 scale study, *Environ. Res. Lett.*, 13, 015006, <https://doi.org/10.1088/1748-9326/aa9938>, 2018.

1259 Hay, L. E. and McCabe, G. J.: Hydrologic effects of climate change in the Yukon River Basin, *Clim. Change*,
1260 100, 509–523, <https://doi.org/10.1007/s10584-010-9805-x>, 2010.

- 1261 Hewitson, B. C., Daron, J., Crane, R. G., Zermoglio, M. F., and Jack, C.: Interrogating empirical-statistical
1262 downscaling, *Clim. Change*, 122, 539–554, <https://doi.org/10.1007/s10584-013-1021-z>, 2014.
- 1263 Huang, S., Shah, H., Naz, B. S., Shrestha, N., Mishra, V., Daggupati, P., Ghimire, U., and Vetter, T.: Impacts
1264 of hydrological model calibration on projected hydrological changes under climate change—a multi-
1265 model assessment in three large river basins, *Clim. Change*, 163, 1143–1164,
1266 <https://doi.org/10.1007/s10584-020-02872-6>, 2020.
- 1267 Hundecha, Y., Arheimer, B., Berg, P., Capell, R., Musuuza, J., Pechlivanidis, I., and Photiadou, C.: Effect of
1268 model calibration strategy on climate projections of hydrological indicators at a continental scale, *Clim.*
1269 *Change*, 163, 1287–1306, <https://doi.org/10.1007/s10584-020-02874-4>, 2020.
- 1270 Islam, S. U., Curry, C. L., Déry, S. J., and Zwiers, F. W.: Quantifying projected changes in runoff variability
1271 and flow regimes of the Fraser River Basin, *British Columbia, Hydrol. Earth Syst. Sci.*, 23, 811–828,
1272 <https://doi.org/10.5194/hess-23-811-2019>, 2019.
- 1273 Ismail, H., Rowshon, M. K., Hin, L. S., Abdullah, A. F. B., and Nasidi, N. M.: Assessment of climate change
1274 impact on future streamflow at Bernam river basin Malaysia, *IOP Conf. Ser. Earth Environ. Sci.*, 540,
1275 012040, <https://doi.org/10.1088/1755-1315/540/1/012040>, 2020.
- 1276 Kourzeneva, E., Asensio, H., Martin, E., and Faroux, S.: Global gridded dataset of lake coverage and lake
1277 depth for use in numerical weather prediction and climate modelling, *Tellus Dyn. Meteorol. Oceanogr.*,
1278 <https://doi.org/10.3402/tellusa.v64i0.15640>, 2012.
- 1279 Krysanova, V., Vetter, T., Eisner, S., Huang, S., Pechlivanidis, I., Michael Strauch, Gelfan, A., Kumar, R.,
1280 Aich, V., Arheimer, B., Chamorro, A., Griensven, A. van, Kundu, D., Lobanova, A., Mishra, V., Plötner, S.,
1281 Reinhardt, J., Ousmane Seidou, Wang, X., Wortmann, M., Zeng, X., and Hattermann, F. F.:
1282 Intercomparison of regional-scale hydrological models and climate change impacts projected for 12
1283 large river basins worldwide—a synthesis, *Environ. Res. Lett.*, 12, 105002, <https://doi.org/10.1088/1748->
1284 [9326/aa8359](https://doi.org/10.1088/1748-9326/aa8359), 2017.
- 1285 Krysanova, V., Zaherpour, J., Didovets, I., Gosling, S. N., Gerten, D., Hanasaki, N., Müller Schmied, H.,
1286 Pokhrel, Y., Satoh, Y., Tang, Q., and Wada, Y.: How evaluation of global hydrological models can help to
1287 improve credibility of river discharge projections under climate change, *Clim. Change*, 163, 1353–1377,
1288 <https://doi.org/10.1007/s10584-020-02840-0>, 2020.
- 1289 L. Sushama, R. Laprise, D. Caya, A. Frigon, and M. Slivitzky: Canadian RCM projected climate-change
1290 signal and its sensitivity to model errors, *Int J Clim.*, 26, 2141–2159, 2006.
- 1291 Lange, S.: Trend-preserving bias adjustment and statistical downscaling with ISIMIP3BASD (v1. 0),
1292 *Geosci. Model Dev.*, 12, 2019.
- 1293 MacDonald, M. K., Stadnyk, T. A., Déry, S. J., Braun, M., Gustafsson, D., Isberg, K., and Arheimer, B.:
1294 Impacts of 1.5 and 2.0 °C Warming on Pan-Arctic River Discharge Into the Hudson Bay Complex Through
1295 2070, *Geophys. Res. Lett.*, 45, 7561–7570, <https://doi.org/10.1029/2018GL079147>, 2018.
- 1296 Manning, R.: On the flow of water in open channels and pipes, *Trans. Inst. Civ. Eng. Irel.*, XX, 161–207,
1297 1891.

- 1298 Maraun, D.: Bias Correcting Climate Change Simulations - a Critical Review, *Curr. Clim. Change Rep.*, 2,
1299 211–220, <https://doi.org/10.1007/s40641-016-0050-x>, 2016.
- 1300 Maraun, D., Shepherd, T. G., Widmann, M., Zappa, G., Walton, D., Gutiérrez, J. M., Hagemann, S.,
1301 Richter, I., Soares, P. M. M., Hall, A., and Mearns, L. O.: Towards process-informed bias correction of
1302 climate change simulations, *Nat. Clim. Change*, 7, 764–773, <https://doi.org/10.1038/nclimate3418>,
1303 2017.
- 1304 Miller, J. R. and Russell, G. L.: The impact of global warming on river runoff, *J. Geophys. Res.*
1305 *Atmospheres*, 97, 2757–2764, <https://doi.org/10.1029/91JD01700>, 1992.
- 1306 Miller, O. L., Putman, A. L., Alder, J., Miller, M., Jones, D. K., and Wise, D. R.: Changing climate drives
1307 future streamflow declines and challenges in meeting water demand across the southwestern United
1308 States, *J. Hydrol. X*, 11, 100074, <https://doi.org/10.1016/j.hydroa.2021.100074>, 2021.
- 1309 Moss, R. H., Edmonds, J. A., Hibbard, K. A., Manning, M. R., Rose, S. K., van Vuuren, D. P., Carter, T. R.,
1310 Emori, S., Kainuma, M., Kram, T., Meehl, G. A., Mitchell, J. F. B., Nakicenovic, N., Riahi, K., Smith, S. J.,
1311 Stouffer, R. J., Thomson, A. M., Weyant, J. P., and Wilbanks, T. J.: The next generation of scenarios for
1312 climate change research and assessment, *Nature*, 463, 747–756, <https://doi.org/10.1038/nature08823>,
1313 2010.
- 1314 Oki, T. and Sud, Y. C.: Design of Total Runoff Integrating Pathways (TRIP)—A Global River Channel
1315 Network, *Earth Interact.*, 2, 1–37, [https://doi.org/10.1175/1087-3562\(1998\)002<0001:DOTRIP>2.3.CO;2](https://doi.org/10.1175/1087-3562(1998)002<0001:DOTRIP>2.3.CO;2),
1316 1998.
- 1317 Poitras, V., Sushama, L., Seglenieks, F., Khaliq, M. N., and Soulis, E.: Projected Changes to Streamflow
1318 Characteristics over Western Canada as Simulated by the Canadian RCM, *J. Hydrometeorol.*, 12, 1395–
1319 1413, <https://doi.org/10.1175/JHM-D-10-05002.1>, 2011.
- 1320 Prowse, T. D.: Ice jam characteristics, Liard–Mackenzie rivers confluence, *Can. J. Civ. Eng.*, 13, 653–665,
1321 <https://doi.org/10.1139/l86-100>, 1986.
- 1322 Quinn, F. H.: Hydraulic Residence Times for the Laurentian Great Lakes, *J. Gt. Lakes Res.*, 18, 22–28,
1323 [https://doi.org/10.1016/S0380-1330\(92\)71271-4](https://doi.org/10.1016/S0380-1330(92)71271-4), 1992.
- 1324 Salathé, E. P., Leung, L. R., Qian, Y., and Zhang, Y.: Regional climate model projections for the State of
1325 Washington, *Clim. Change*, 102, 51–75, <https://doi.org/10.1007/s10584-010-9849-y>, 2010.
- 1326 von Salzen, K., Scinocca, J. F., McFarlane, N. A., Li, J., Cole, J. N. S., Plummer, D., Verseghy, D., Reader, M.
1327 C., Ma, X., Lazare, M., and Solheim, L.: The Canadian Fourth Generation Atmospheric Global Climate
1328 Model (CanAM4). Part I: Representation of Physical Processes, *Atmosphere-Ocean*, 51, 104–125,
1329 <https://doi.org/10.1080/07055900.2012.755610>, 2013.
- 1330 Schlund, M., Lauer, A., Gentine, P., Sherwood, S. C., and Eyring, V.: Emergent constraints on equilibrium
1331 climate sensitivity in CMIP5: do they hold for CMIP6?, *Earth Syst. Dyn.*, 11, 1233–1258,
1332 <https://doi.org/10.5194/esd-11-1233-2020>, 2020.
- 1333 Schnorbus, M., Werner, A., and Bennett, K.: Impacts of climate change in three hydrologic regimes in
1334 British Columbia, Canada, *Hydrol. Process.*, 28, 1170–1189, <https://doi.org/10.1002/hyp.9661>, 2014.

1335 Scinocca, J. F., Kharin, V. V., Jiao, Y., Qian, M. W., Lazare, M., Solheim, L., Flato, G. M., Biner, S.,
1336 Desgagne, M., and Dugas, B.: Coordinated Global and Regional Climate Modeling, *J. Clim.*, 29, 17–35,
1337 <https://doi.org/10.1175/JCLI-D-15-0161.1>, 2016.

1338 Shi, H., Li, T., and Wei, J.: Evaluation of the gridded CRU TS precipitation dataset with the point
1339 raingauge records over the Three-River Headwaters Region, *J. Hydrol.*, 548, 322–332,
1340 <https://doi.org/10.1016/j.jhydrol.2017.03.017>, 2017.

1341 Shrestha, R. R., Schnorbus, M. A., Werner, A. T., and Berland, A. J.: Modelling spatial and temporal
1342 variability of hydrologic impacts of climate change in the Fraser River basin, British Columbia, Canada,
1343 *Hydrol. Process.*, 26, 1840–1860, <https://doi.org/10.1002/hyp.9283>, 2012.

1344 Shrestha, R. R., Cannon, A. J., Schnorbus, M. A., and Alford, H.: Climatic Controls on Future Hydrologic
1345 Changes in a Subarctic River Basin in Canada, *J. Hydrometeorol.*, 20, 1757–1778,
1346 <https://doi.org/10.1175/JHM-D-18-0262.1>, 2019.

1347 Shrestha, R. R., Bonsal, B. R., Bonnyman, J. M., Cannon, A. J., and Najafi, M. R.: Heterogeneous snowpack
1348 response and snow drought occurrence across river basins of northwestern North America under 1.0°C
1349 to 4.0°C global warming, *Clim. Change*, 164, 40, <https://doi.org/10.1007/s10584-021-02968-7>, 2021a.

1350 Shrestha, R. R., Bonsal, B. R., Kayastha, A., Dibike, Y. B., and Spence, C.: Snowpack response in the
1351 Assiniboine-Red River basin associated with projected global warming of 1.0 °C to 3.0 °C, *J. Gt. Lakes
1352 Res.*, 47, 677–689, <https://doi.org/10.1016/j.jglr.2020.04.009>, 2021b.

1353 Sobie, S. R. and Murdock, T. Q.: Projections of Snow Water Equivalent Using a Process-Based Energy
1354 Balance Snow Model in Southwestern British Columbia, *J. Appl. Meteorol. Climatol.*, 61, 77–95,
1355 <https://doi.org/10.1175/JAMC-D-20-0260.1>, 2022.

1356 Stadnyk, T. A., Tefs, A., Broesky, M., Déry, S. J., Myers, P. G., Ridenour, N. A., Koenig, K., Vonderbank, L.,
1357 and Gustafsson, D.: Changing freshwater contributions to the Arctic: A 90-year trend analysis (1981–
1358 2070), *Elem. Sci. Anthr.*, 9, <https://doi.org/10.1525/elementa.2020.00098>, 2021.

1359 Sun, Q., Miao, C., Duan, Q., Ashouri, H., Sorooshian, S., and Hsu, K.-L.: A Review of Global Precipitation
1360 Data Sets: Data Sources, Estimation, and Intercomparisons, *Rev. Geophys.*, 56, 79–107,
1361 <https://doi.org/10.1002/2017RG000574>, 2018.

1362 Swart, N. C., Cole, J. N. S., Kharin, V. V., Lazare, M., Scinocca, J. F., Gillett, N. P., Anstey, J., Arora, V.,
1363 Christian, J. R., Hanna, S., Jiao, Y., Lee, W. G., Majaess, F., Saenko, O. A., Seiler, C., Seinen, C., Shao, A.,
1364 Sigmund, M., Solheim, L., von Salzen, K., Yang, D., and Winter, B.: The Canadian Earth System Model
1365 version 5 (CanESM5.0.3), *Geosci. Model Dev.*, 12, 4823–4873, [https://doi.org/10.5194/gmd-12-4823-
1366 2019](https://doi.org/10.5194/gmd-12-4823-2019), 2019.

1367 Thrasher, B., Xiong, J., Wang, W., Melton, F., Michaelis, A., and Nemani, R.: Downscaled Climate
1368 Projections Suitable for Resource Management, *Eos Trans. Am. Geophys. Union*, 94, 321–323,
1369 <https://doi.org/10.1002/2013EO370002>, 2013.

1370 Trenberth, K. E., Smith, L., Qian, T., Dai, A., and Fasullo, J.: Estimates of the Global Water Budget and Its
1371 Annual Cycle Using Observational and Model Data, *J. Hydrometeorol.*, 8, 758–769,
1372 <https://doi.org/10.1175/JHM600.1>, 2007.

1373 Versegby, D. L.: Class—A Canadian land surface scheme for GCMS. I. Soil model, *Int. J. Climatol.*, **11**,
1374 111–133, <https://doi.org/10.1002/joc.3370110202>, 1991.

1375 Versegby, D. L., McFarlane, N. A., and Lazare, M.: Class—A Canadian land surface scheme for GCMS, II.
1376 Vegetation model and coupled runs, *Int. J. Climatol.*, **13**, 347–370,
1377 <https://doi.org/10.1002/joc.3370130402>, 1993.

1378 Werner, A. T., Schnorbus, M. A., Shrestha, R. R., Cannon, A. J., Zwiers, F. W., Dayon, G., and Anslow, F.: A
1379 long-term, temporally consistent, gridded daily meteorological dataset for northwestern North America,
1380 *Sci. Data*, **6**, 180299, <https://doi.org/10.1038/sdata.2018.299>, 2019.

1381 Winter, J. M. and Eltahir, E. A. B.: Modeling the hydroclimatology of the midwestern United States. Part
1382 2: future climate, *Clim. Dyn.*, **38**, 595–611, <https://doi.org/10.1007/s00382-011-1183-1>, 2012.

1383 Wong, J. S., Razavi, S., Bonsal, B. R., Wheeler, H. S., and Asong, Z. E.: Inter-comparison of daily
1384 precipitation products for large-scale hydro-climatic applications over Canada, *Hydrol. Earth Syst. Sci.*,
1385 **21**, 2163–2185, <https://doi.org/10.5194/hess-21-2163-2017>, 2017.

1386 Yoosefdoost, I., Khashei-Siuki, A., Tabari, H., and Mohammadrezapour, O.: Runoff Simulation Under
1387 Future Climate Change Conditions: Performance Comparison of Data-Mining Algorithms and Conceptual
1388 Models, *Water Resour. Manag.*, **36**, 1191–1215, <https://doi.org/10.1007/s11269-022-03068-6>, 2022.

1389 Zhang, X., Tang, Q., Zhang, X., and Lettenmaier, D. P.: Runoff sensitivity to global mean temperature
1390 change in the CMIP5 Models, *Geophys. Res. Lett.*, **41**, 5492–5498,
1391 <https://doi.org/10.1002/2014GL060382>, 2014.

1392

1393